# Experiments on the $2^3P$ State of Helium. I. A Measurement of the $2^3P_1$-$2^3P_2$ Fine Structure*

F. M. J. PICHANICK, R. D. SWIFT,† C. E. JOHNSON,‡ AND V. W. HUGHES
*Physics Department, Yale University, New Haven, Connecticut 06520*
(Received 4 December 1967)

A measurement, accurate to 3 ppm, is reported of the $2^3P_1$-$2^3P_2$ fine structure in $He^4$. An atomic-beam optical-microwave resonance technique was used. Two sets of measurements were made on the transition $2^3P_1(m_J=0)\leftrightarrow 2^3P_2(m_J=0)$. The first set was in a magnetic field of about 100 G ("low" field), where the uncertainties arose from field-dependent asymmetries in the line shape. The second set of measurements was in a field of about 500 G ("high" field), and here the main uncertainties were in the field measurements and the calculation of $g$ factors. The results of the two sets were in good agreement: low field: $E(2^3P_1)$-$E(2^3P_2)$ $=2291.188\pm0.015$ MHz; high field: $E(2^3P_1)$-$E(2^3P_2)=2291.197\pm0.008$ MHz; weighted mean: $E(2^3P_1)$-$E(2^3P_2)=2291.195\pm0.007$ MHz. The advantages of the atomic-beam technique and the possible importance of this fine-structure measurement are discussed.

## I. INTRODUCTION

THE study of quantum electrodynamics depends to a large extent on the experimental and theoretical analysis of simple atomic systems for which detailed calculations are feasible. High-precision measurements of the fine structure and hyperfine structure of hydrogen and deuterium,[1] singly ionized helium,[2] positronium,[3] and muonium[4] have therefore been the subject of much experimental research. These experiments are also important in evaluating the fine-structure constant $\alpha(=e^2/\hbar c)$.

Experimental work on helium—in particular, measurement of its fine-structure intervals—has not yet been done to the precision achieved for the single-electron atoms. Helium is a simple enough atom so that it may be possible to calculate its fine-structure intervals reliably to the precision with which they can be measured, which is of the order of 1 part per million (ppm). Comparison of experimental and theoretical values of helium fine-structure intervals accurate to a precision of 1 ppm would provide a valuable test of the theory of the electron-electron interaction. It would also provide a new determination of the value of the fine-structure constant $\alpha$ to a precision considerably higher than is presently known.

Values of the fine-structure constant $\alpha$ are presently determined from measurements of deuterium fine structure,[1] muonium hyperfine structure,[4] hydrogen hyperfine structure,[5] and the ac Josephson effect.[6] The precision of these determinations is between about 5 and 10 ppm (1 standard deviation). All four values are not in satisfactory agreement. Hence, it is of great importance to determine $\alpha$ by another method and with higher precision. Study of the fine structure of helium is a promising method of determining $\alpha$ to a precision of about 1 ppm.

In this paper we report a precision measurement of the fine-structure interval $J=1$ to 2 for the $2^3P$ state of He. In a later paper a measurement of the interval $J=0$ to 1 will be reported. Since the ratio of the radiative linewidth to the fine-structure intervals is between $\frac{1}{10}$ and 1/100 the corresponding ratio for the $2^2P_{3/2}$-to-$2^2P_{1/2}$ fine-structure interval of hydrogen due to the relatively long lifetime ($\sim10^{-7}$ sec) of the $2^3P$ state of He, determination of the helium fine-structure intervals to a precision greater than that of hydrogen can be achieved. Preliminary reports of the results of this experiment have been given.[7]

The method used in the present experiment is the optical-rf atomic-beam magnetic-resonance method,[8] which was first developed and applied to measure hyperfine structure in an optically excited state of $Na^{23}$. The method permits the measurement of magnetic-resonance transitions in short-lived optically excited states by observing the effect of such transitions on the magnetic sublevel populations of a stable atomic beam. In our case this was a beam of helium atoms in the $2^3S_1$ metastable state (Fig. 1). The atomic-beam

* Research reported in this publication was supported in part by the Advanced Research Project Agency under Grant No. AF49(638)545, and the U. S. Air Force Office of Scientific Research under Grants Nos. AFOSR 249-62, 249-63, 249-64, and 249-65.

† Present address: American Science and Engineering, Inc., 11 Carleton Street, Cambridge, Mass.

‡ Present address: Department of Physics, University of California, Berkeley, Calif.

[1] S. Triebwasser, E. S. Dayhoff, and W. E. Lamb, Jr., Phys. Rev. **89**, 98 (1953); E. S. Dayhoff, S. Triebwasser, and W. E. Lamb, Jr., *ibid.* **89**, 106 (1953).

[2] E. Lipworth and R. Novick, Phys. Rev. **108**, 1434 (1957).

[3] R. Weinstein, M. Deutsch, and S. C. Brown, Phys. Rev. **98**, 223 (1955); V. W. Hughes, S. Marder, and C. S. Wu, *ibid.* **106**, 934 (1957); E. D. Theriot, R. H. Beers, and V. W. Hughes, Phys. Rev. Letters **18**, 767 (1967).

[4] W. E. Cleland *et al.*, Phys. Rev. Letters **13**, 202 (1964); P. Thompson *et al.*, Bull. Am. Phys. Soc. **12**, 75 (1967); V. W. Hughes, Ann. Rev. Nucl. Sci. **16**, 445 (1966).

[5] S. B. Crampton, D. Kleppner, and N. Ramsey, Phys. Rev. Letters **11**, 338 (1963) (experimental measurement of hydrogen hyperfine structure); S. D. Drell and J. D. Sullivan, Phys. Rev. **154**, 1477 (1967) (most recent discussion of the theoretical hyperfine structure).

[6] W. H. Parker, B. N. Taylor, and D. N. Langenberg, Phys. Rev. Letters **18**, 287 (1967).

[7] F. M. J. Pichanick, R. D. Swift, and V. W. Hughes, Bull. Am. Phys. Soc. **9**, 90 (1964); R. D. Swift, F. M. J. Pichanick, and V. W. Hughes, *ibid.* **10**, 455 (1965).

[8] M. L. Perl, I. I. Rabi, and B. Senitsky, Phys. Rev. **98**, 611 (1955); B. B. Aubrey, L. Y. Chow, V. W. Hughes, and R. Swift, Bull. Am. Phys. Soc. **6**, 248 (1961); see also P. Kusch and V. W. Hughes, in *Encyclopaedia of Physics*, edited by S. Flügge (Springer-Verlag, Berlin, 1959), Vol. 37/1.

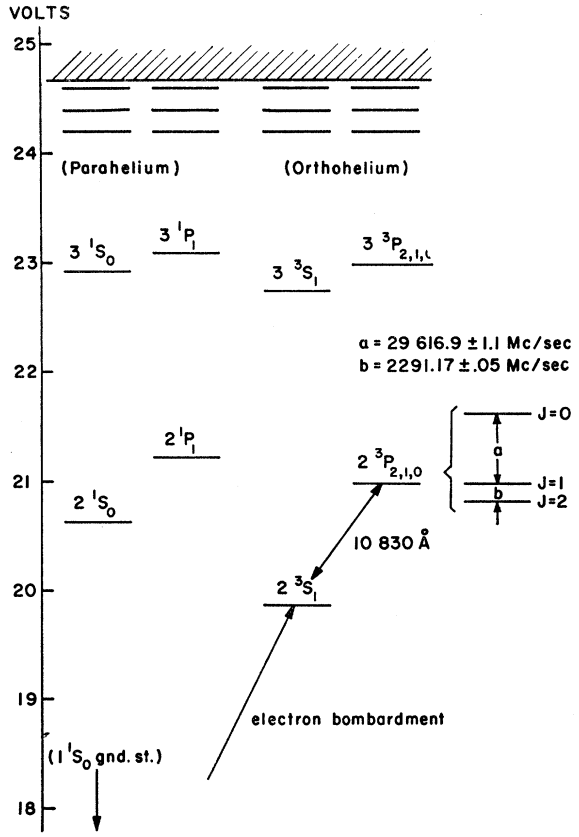


FIG. 1. Energy-level diagram of the helium atom. The $1^1S_0$ ground state, which lies 19.82 eV below the metastable $2^3S$ state, has been omitted. The $2^3P$ fine structure (not to scale) is shown in detail.

method has the important advantage of allowing study of the free atom, uncomplicated by collisional effects, and magnetic-resonance transitions may be observed at any value of the applied magnetic field.

Early measurements of helium fine structure in the $2^3P$ state were done by optical spectroscopy[9] with an accuracy of about 1%. The first precision measurement using microwave spectroscopy was done by Lamb and his associates at Stanford.[10] In their experiment the $2^3P$ state was produced with a net magnetic polarization by electron bombardment in a particular direction, and microwave-induced magnetic-resonance transitions between fine-structure levels were observed through the accompanying changes in intensity and polarization of the $2^3P \rightarrow 2^3S$ optical radiation. Fine-structure measurements were made to an accuracy of about 150 ppm. Recently the optical method of level-crossing has been applied to the measurement of the $2^3P$ fine structure and results to an accuracy of about 10 ppm have been reported.[11] The level-crossing technique does not permit separate measurements, comparable in accuracy, of both the fine structure and the $g$ factors.

An evaluation of $\alpha$ to a precision of 1 ppm from the measured fine structure of the $2^3P$ state of helium would require theoretical calculations of comparable accuracy. Accurate nonrelativistic variational wave functions have been obtained recently,[12] and the Breit interaction terms[13] of order $\alpha^2$ Ry were computed to the relevant accuracy. An "anomalous-electron-moment" term of order $\alpha^3$ Ry was included. A calculation of terms of order $\alpha^4$ Ry due to relativistic and radiative corrections must also be made. A preliminary estimate of some of these terms has been published.[14]

## II. THEORY OF THE EXPERIMENT

### A. Energy Levels

The Zeeman Hamiltonian for the $2^3P$ states in helium has been treated by Lamb.[15] It can be written in the form

$$\mathcal{H}=\mathcal{H}_{fs}+g_s\mu_0\mathbf{S}\cdot\mathbf{H}+g_L\mu_0\mathbf{L}\cdot\mathbf{H}=\mathcal{H}_{fs}+g_s\mu_0 S_zH+g_L\mu_0L_zH, \quad (1)$$

where $g_L=1$, $g_s=2.00232$. $H$ is the uniform magnetic field assumed to be in the $z$ direction, $\mu_0$ the Bohr magneton, and $g_s$, $g_L$ are, respectively, the usual electronic spin and orbital $g$ factors. $\mathbf{L}$ and $\mathbf{s}$, respectively, are the total orbital and spin angular-momentum operators.

$\mathcal{H}_{fs}$ contains the spin-orbit and spin-spin operators which lead to the fine structure.[13] Since it is diagonal in $\mathbf{J}(=\mathbf{L}+\mathbf{S})$, we shall be concerned only with its eigenvalues $E_J$ in a representation wherein $\mathbf{J}$ is itself diagonal. For the time being we have omitted the relativistic contributions[16] to the Zeeman Hamiltonian. These terms, of order $\alpha^2\mu_0H$, will be considered in a later section. The term $g_L\mu_0L_zH$ assumes that the nucleus is stationary. The effect of nuclear motion has been considered by Philips,[17] who showed that its contribution is proportional to $(m/M)L_z\mu_0H$, where $m$ and $M$ are the respective masses of the electron and nucleus. The motional effect can therefore be included as a correction of order $m/M$ to $g_L$ (see Appendix C).

The Zeeman Hamiltonian $\mathcal{H}$ is not diagonal in $J$, owing to the presence of the field-dependent terms.

[9] J. Brochard, R. Chabbal, H. Chantret, and P. Jacquinot, J. Phys. Radium **13**, 433 (1952).
[10] W. E. Lamb, Jr., and T. H. Maiman, Phys. Rev. **105**, 573 (1957); I. Weider and W. E. Lamb, Jr., *ibid.* **107**, 125 (1957).
[11] F. D. Colegrove, P. A. Franken, R. R. Lewis, and R. H. Sands, Phys. Rev. Letters **3**, 420 (1959); J. Lifsitz and R. H. Sands, Bull. Am. Phys. Soc. **10**, 1214 (1965); J. Lifsitz, thesis, University of Michigan, 1965 (unpublished).
[12] C. L. Pekeris, B. Schiff, and H. Lifson, Phys. Rev. **126**, 1057 (1962); B. Schiff, C. L. Pekeris, and H. Lifson, *ibid.* **137**, A1672 (1965); C. Schwartz, *ibid.* **134**, A1181 (1964).
[13] H. A. Bethe and E. E. Salpeter, *Quantum Mechanics of One- and Two-Electron Atoms* (Springer-Verlag, Berlin, 1957), Sec. 40.
[14] K. Y. Kim, Phys. Rev. **140**, A1498 (1965).
[15] W. E. Lamb, Jr., Phys. Rev. **105**, 559 (1957).
[16] W. Perl and V. W. Hughes, Phys. Rev. **91**, 842 (1953); W. Perl, *ibid.* **91**, 852 (1953); A. Abragam and J. H. van Vleck, *ibid.* **92**, 1448 (1953); F. R. Innes and C. W. Ufford, *ibid.* **111**, 194 (1958).
[17] M. Philips, Phys. Rev. **76**, 1803 (1949).

These terms couple states having the same $m_J$, which is the usual quantum number associated with the eigenvalue of $J_z$. It is convenient to set up the Hamiltonian in a representation in which the angular-momentum eigenfunctions $\Psi(J,m_J)$ are the bases. Since $L=S=1$ for a $^3P$ state, the possible values of $J$ are 0, 1, and 2. The matrix representation of $\mathfrak{IC}$ is conveniently written as a set of submatrices, each designating a different value of $m_J$ (Appendix A ,Table II). The energy levels and transition frequencies are obtained by solving the secular equations derived from these submatrices. The energy levels as a function of magnetic field are illustrated in Fig. 2 for $J=1$ and 2.

The allowed magnetic-dipole transitions between the various $^3P(m_J)$ sublevels have been summarized by Lamb.[15] An accurate determination of the $2^3P_1$-$2^3P_2$ fine-structure separation made it desirable to measure the frequency of a $\Delta m_J=0$ transition, since at fairly low magnetic fields this would be independent of field to first order. The frequencies, to second order in the field, of transitions 4 ($\Delta m_J=0$, $m_J=0$) and 5 ($\Delta m_J=0$, $m_J=\pm1$) have been included in Table III (Appendix A), and are illustrated in Fig. 3. Our measurements primarily involved transition 4 since this had a much larger signal strength.

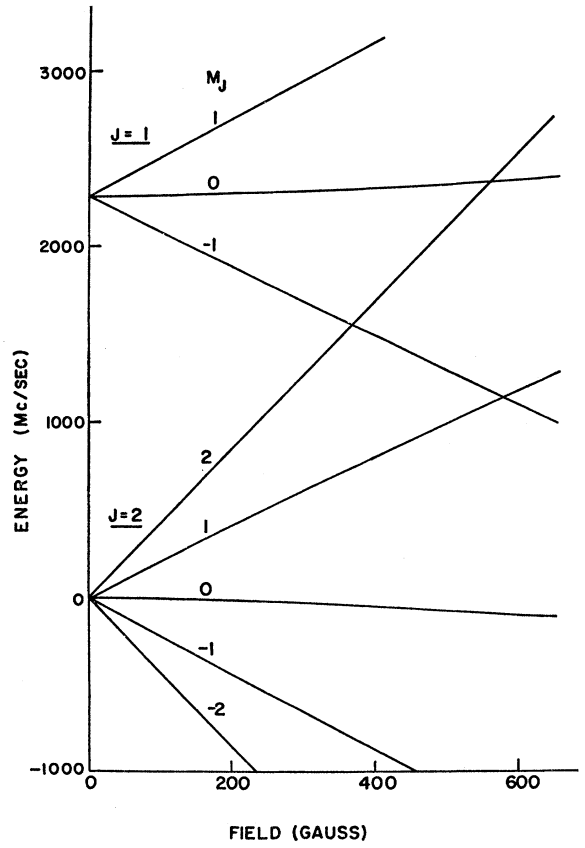


FIG. 2. Variation of the $2^3P_1$ and $2^3P_2$ energy levels as a function of magnetic field. Two observable level crossings (Ref. 11), ($J=2$, $m_J=+2\leftrightarrow J=1$, $m_J=0$) and ($J=2$, $m_J=+1\leftrightarrow J=1$, $m_J=-1$), occur at a field of about 580 G.

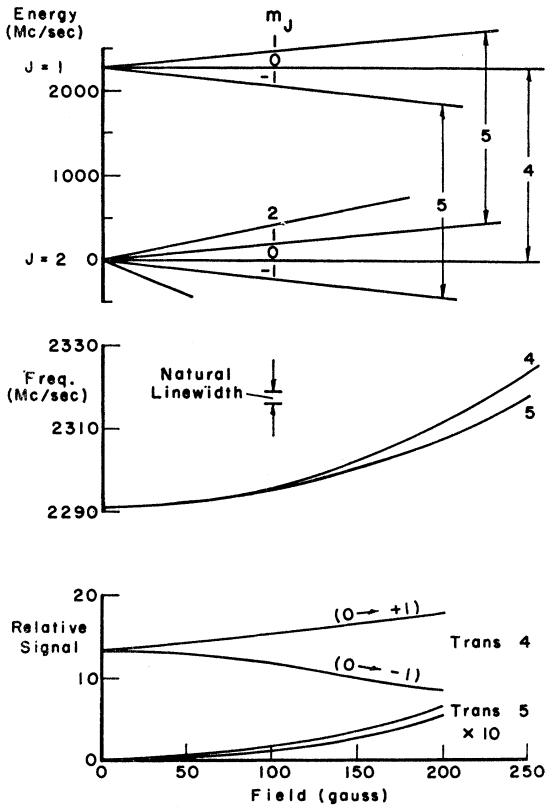


FIG. 3. Magnetic-field-dependent plot of (a) $2^3P_2$, $2^3P_1$ energy levels, illustrating transitions 4 and 5; (b) resonant frequencies of transitions 4 and 5. An indication is given of how their frequency separation compares with their natural linewidth. (c) Relative intensities of transitions 4 and 5 for the $2^3S(m_S)$ ($0\rightarrow+1$) and ($0\rightarrow-1$) trajectories.

### B. Optical Transition Probabilities

At nonzero fields the $2^3P$ eigenfunctions are linear combinations of the $\Psi(J,m_J)$:

$$\Psi(\mathcal{J}m_J)=\sum_{J\geq|m_J|}(Jm_J|\mathcal{J}m_J)\Psi(Jm_J). \qquad (2)$$

This is the convention due to Lamb[15] whereby $\mathcal{J}$ is the value of the quantum number $J$ which would designate the particular $\Psi(\mathcal{J}m_J)$ at zero field. The coefficients $(Jm_J|\mathcal{J}m_J)$ are obtained from the solutions to the secular equations for each $m_J$, and are given to second order in the field in Table III.

The electric-dipole matrix elements are diagonal in $S_z$, and hence it will be convenient to expand the $\Psi(\mathcal{J}m_J)$ as linear combinations of the products $\Phi(m_L)\times\chi(m_S)$, where $\phi(m_L)$ and $\chi(m_S)$ are, respectively, the eigenfunctions of $L_z$ and $S_z$. Using the abbreviated notation $(m_Sm_L|Jm_J)$ for the (Wigner) angular-momentum coupling coefficients $(SLm_Sm_L|SLJm_J)$ we

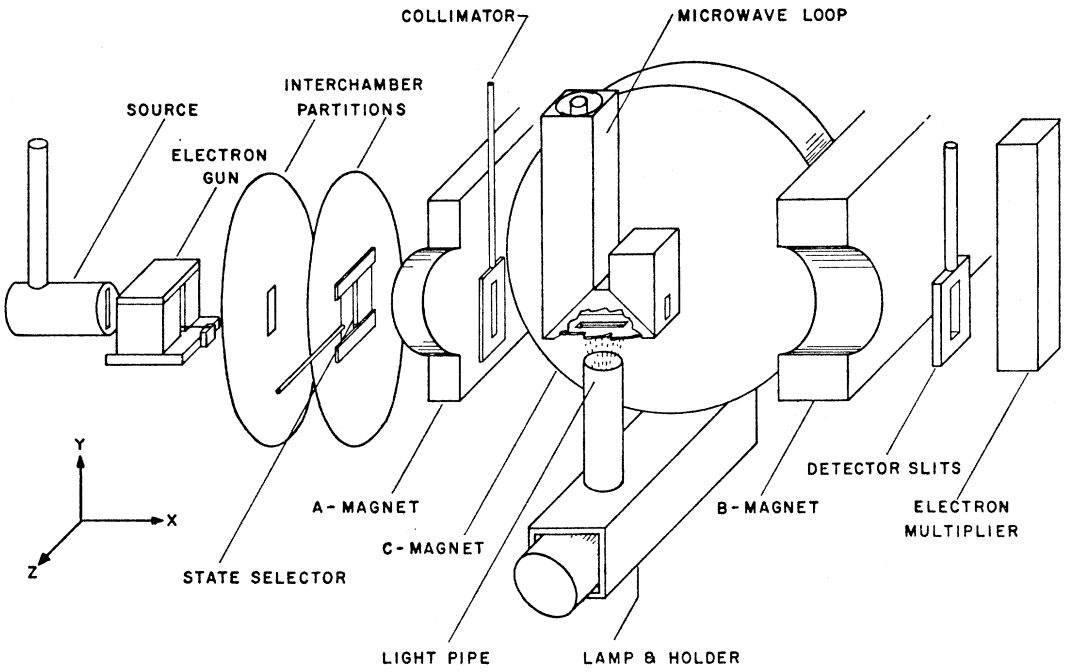


FIG. 4. Over-all diagram of the atomic-beam apparatus.

have

$$\Psi(Jm_J)=\sum_{m_S}(m_Sm_L|Jm_J)\phi(m_L)\chi(m_S), \tag{3}$$

where $m_J=m_L+m_S$. Hence,

$$\begin{aligned}\Psi(\mathcal{J}m_J)&=\sum_{J\geq|m_J|}(Jm_J|\mathcal{J}m_J)\\&\quad\times\{\sum_{m_S}(m_Sm_L|Jm_J)\phi(m_L)\chi(m_S)\}\\&=\sum_{m_S}\{\sum_{J\geq|m_J|}(Jm_J|\mathcal{J}m_J)(m_Sm_L|Jm_J)\\&\quad\times\phi(m_L)\chi(m_S)\}\\&=\sum_{m_S}\{m_Sm_L|\mathcal{J}m_J\}\phi(m_L)\chi(m_S),\end{aligned} \tag{4}$$

where the last two lines serve to define the $\{m_Sm_L|\mathcal{J}m_J\}$. Values of $|\{m_Sm_L|\mathcal{J}m_J\}|^2$ are given, to first order in magnetic field, in Table IV.

The electric-dipole matrix elements are given by

$$(2^3S|\mathbf{r}|2^3P,m_L=\pm1)=R(1s2s|1s2p)(\hat{\imath}+\hat{\jmath})/\sqrt{2}, \tag{5}$$

$$(2^3S|\mathbf{r}|2^3P,m_L=0)=R(1s2s|1s2p)\hat{k}. \tag{6}$$

The radial integral $R(1s2s|1s2p)$ is of no further interest since we are concerned only with the relative values of the electric-dipole matrix elements. $\hat{\imath}$, $\hat{\jmath}$, $\hat{k}$ are unit vectors in the $x$, $y$, $z$ directions, respectively.

Equations (5) and (6) are proportional to the amplitudes for spontaneous decay from the $2^3P$ state, for light polarized in the specified directions. The $C$ field defined the $z$ direction in our apparatus, and the exciting radiation was assumed to be a plane wave traveling in the $y$ direction, with polarization uniformly distributed in the $xz$ plane (see Fig. 4). Let the spectral intensities for excitation of the transition $2^3S\rightarrow2^3P(\mathcal{J})$ be $I(\mathcal{J})$. Then the excitation amplitudes are proportional to

$$\begin{aligned}\theta(\mathcal{J},m_L=\pm1)&=[I(\mathcal{J})]^{1/2}R(1s2s|1s2p)\hat{\imath}/\sqrt{2}\\&\qquad\text{for}\quad 2^3S\rightarrow2^3P,\ m_L=\pm1,\\\theta(\mathcal{J},m_L=0)&=[I(\mathcal{J})]^{1/2}R(1s2s|1s2p)\hat{k}\\&\qquad\text{for}\quad 2^3S\rightarrow2^3P,\ m_L=0.\end{aligned} \tag{7}$$

Finally the optical transition probabilities between the $2^3S(m_S)$ and the $2^3P(\mathcal{J},m_J)$ states are obtained from Eqs. (4)–(7). Assuming suitable multiplicative constants, we have

$$\begin{aligned}\sigma(m_S;\mathcal{J},m_J)&=\{m_S,m_J-m_S|\mathcal{J},m_J\}^2\\&\quad\times|\theta(\mathcal{J},m_L=m_J-m_S)|^2,\\\gamma(\mathcal{J},m_J;m_S')&=\{m_S,m_J-m_S'|\mathcal{J},m_J\}^2\\&\quad\times|(2^3S|\mathbf{r}|2^3P_{\mathcal{J}}m_L=m_J-m_S)|^2,\end{aligned} \tag{8}$$

where $\sigma(m_S;\mathcal{J},m_J)$ and $\gamma(\mathcal{J},m_J;m_S')$ are, respectively, the relative probabilities for excitation from $2^3S(m_S)$ to $2^3P(\mathcal{J},m_J)$ and for decay from $2^3P(\mathcal{J},m_J)$ to $2^3S(m_S')$. We have made explicit use of the fact that the electric-dipole matrices are diagonal in $m_S$. The values of these relative probabilities, at zero magnetic field, are illustrated in Fig. 5.

### C. Signal Strengths

We wish to calculate the probability $P(m_S\rightarrow m_S')$ that an atom, originating in a substate $2^3S(m_S)$, transfers to a substate $2^3S(m_S')$, after a single process of excitation to the $2^3P$ state, followed by radiative decay.

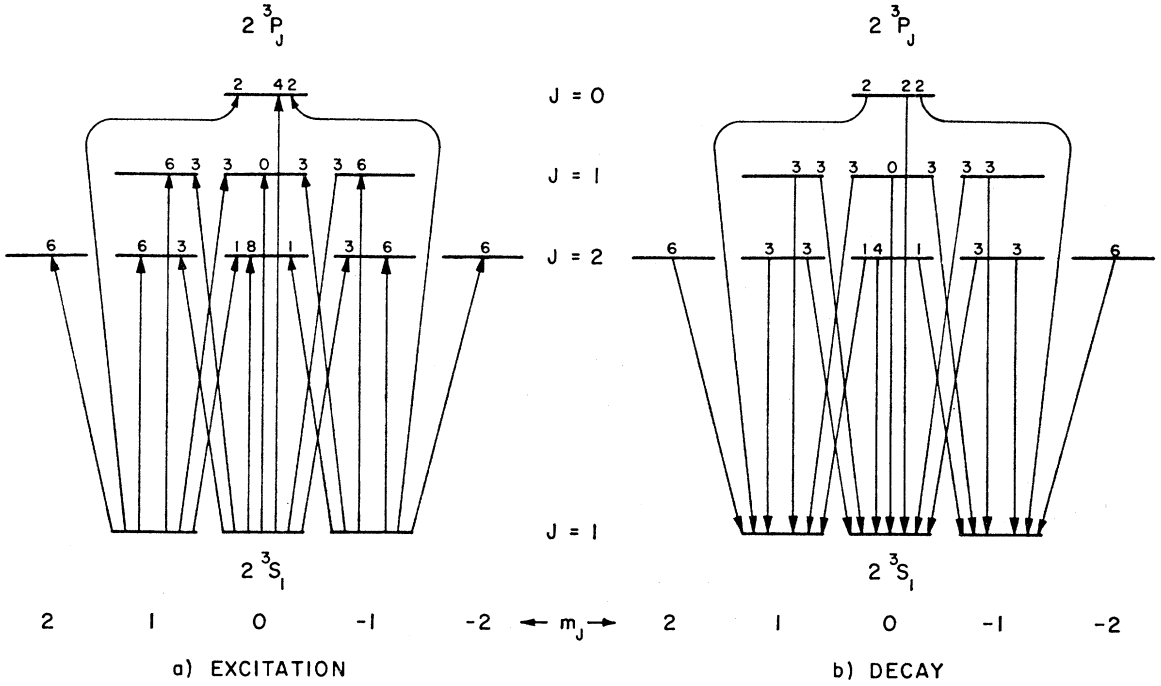


FIG. 5. Relative optical intensities, at zero magnetic field, for the transition $2^3S \leftrightarrow 2^3P$: (a) for excitation by a plane wave incident perpendicular to the axis of quantization, and (b) for isotropic decay.

Transitions between the $2^3P$ and $1^1S_0$ states are forbidden, and we need only consider the decay process which returns the atom to the $2^3S$ state. Hence, we may write

$$P(m_S \to m_S') = \frac{1}{\sum_{\mathcal{J}',m_J'} \sigma(m_S;\mathcal{J}',m_J')} \times \sum_{\mathcal{J},m_J} \frac{\sigma(m_S;\mathcal{J},m_J)\gamma(\mathcal{J},m_J;m_S')}{\sum_{m_S''} \gamma(\mathcal{J},m_J;m_S'')}. \quad (9)$$

The $(\mathcal{J},m_J)$ are the intermediate $2^3P$ substates which may have been excited. Suppose that two of the $(\mathcal{J},m_J)$ labelled $\alpha$, $\beta$ are admixed by a magnetic-resonance transition such that there is a probability $\rho(\alpha,\beta)$ that the atom originally excited to $\alpha$ will decay from $\beta$. A probability $\rho(\beta,\alpha)$ representing a transfer from $\beta$ to $\alpha$ is assumed to exist simultaneously, with $\rho(\alpha,\beta)=\rho(\beta,\alpha)$. The existence of this admixture changes $P(m_S \to m_S')$ to $P'(m_S \to m_S')$ given by

$$P'(m_S \to m_S') = P(m_S \to m_S') + \frac{\rho(\alpha,\beta)}{\sum_{\mathcal{J}'m_J'} \sigma(m_S;\mathcal{J}'m_J')} \times \left\{ \frac{[\sigma(m_S;\beta)-\sigma(m_S;\alpha)]\gamma(\alpha;m_S')}{\sum_{m_S''} \gamma(\alpha;m_S'')} + \frac{[\sigma(m_S;\alpha)-\sigma(m_S;\beta)]\gamma(\beta;m_S')}{\sum_{m_S''} \gamma(\beta;m_S'')} \right\}. \quad (10)$$

An atom in either $\alpha$ or $\beta$ can only decay to one of the $m_S''$, and hence

$$\sum_{m_S''} \gamma(\alpha;m_S'') = \sum_{m_S''} (\beta;m_S'') = 1. \quad (11)$$

Substitution of (11) into (10) yields

$$P'(m_S \to m_S') = P(m_S \to m_S') + \frac{\rho(\alpha,\beta)}{\sum_{\mathcal{J}'m_J'} \sigma(m_S;\mathcal{J}'m_J')} \times [\sigma(m_S;\beta)-\sigma(m_S;\alpha)] \times [\gamma(\alpha;m_S')-\gamma(\beta;m_S')]. \quad (12)$$

In our experiment the observable signal due to the $\alpha \leftrightarrow \beta$ transition was a fractional change in $P(m_S \to m_S')$:

$$S\begin{pmatrix} \alpha & \leftrightarrow \beta \\ m_S \to & m_S' \end{pmatrix} = \frac{P'(m_S \to m_S') - P(m_S \to m_S')}{P(m_S \to m_S')}. \quad (13)$$

A nonzero signal requires, therefore, that

$$\sigma(m_S;\beta) \neq \sigma(m_S;\alpha), \quad \gamma(\alpha;m_S') \neq \gamma(\beta;m_S') \quad (14)$$

for a given set of substates $m_S$, $m_S'$, $\alpha$, $\beta$.

The arrangement of our apparatus was such as to observe the trajectories of atoms originating in the $2^3S(m_S=0)$ substate, and arriving at the detector in either the $2^3S(m_S'=+1)$ or $2^3S(m_S'=-1)$ substates. Substituting (8) into (9), we have for the transition

probabilities

$$P(0\rightarrow\pm1)\propto\sum_{\mathcal{J}} I(\mathcal{J})[\{0\,0|\mathcal{J}\,0\}^2\{\pm1\mp1|\mathcal{J}\,0\}^2 +\tfrac{1}{2}\{0\,\pm1|\mathcal{J}\,\pm1\}^2\{\pm1\,0|\mathcal{J}\,\pm1\}^2]. \quad (15)$$

At present we are concerned with a magnetic resonance in transition 4, where $\alpha$, $\beta$ are the states $2^3P_2$ ($m_J=0$) and $2^3P_1(m_J=0)$. For this transition we have from (12)

$$P'(0\rightarrow\pm1)\propto P(0\rightarrow\pm1)+\rho(\alpha,\beta)[I(\mathcal{J}=1)\{0\,0|1\,0\}^2 -I(\mathcal{J}=2)\{0\,0|2\,0\}^2][\{\pm1\,\mp1|2\,0\}^2 -\{\pm1\,\mp1|1\,0\}^2], \quad (16)$$

From Table IV the relative signal due to transition 4 is given, to first order in field, by

$$S(0\rightarrow\pm1)=\frac{P'(0\rightarrow\pm1)-P(0\rightarrow\pm1)}{P(0\rightarrow\pm1)} =\frac{2\rho(\alpha,\beta)\left\{1\pm\frac{2\mu_0H}{(E_1-E_2)}\mp\frac{2\mu_0H}{(E_0-E_1)}\right\}}{R\left\{1\pm\frac{2\mu_0H}{(E_0-E_1)}\right\}+\left\{1\mp\frac{2\mu_0H}{(E_1-E_2)}\right\}+\frac{9}{4}}. \quad (17)$$

It has been assumed that the ratios $I(\mathcal{J}=2):I(\mathcal{J}=1):I(\mathcal{J}=0)$ are $1:1:R$. This is based on an assumed spectral distribution of the discharge lamp as shown in Fig. 6. The emission lines $2^3P_2\rightarrow2^3S$ and $2^3P_1\rightarrow2^3S$ were not resolved, and lay in positions of roughly equal intensity of the spectral diagram. It can be seen from Fig. 6 that $R$ has a value in the region of 0.4.

$E_2$, $E_1$, and $E_0$ are, respectively, the zero-field energy eigenvalues of the $J=2$, 1, and 0 levels. $(E_0-E_1)$ is larger than $(E_1-E_2)$ by a factor of about 12, and hence

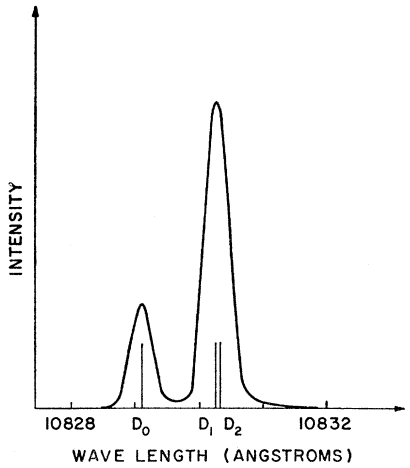


FIG. 6. Relative spectral intensity (as a function of wavelength) for a typical helium discharge lamp used in the experiment. The points $D_0$, $D_1$, and $D_2$ correspond to the energy-level separation between $2^3S$, and $2^3P_0$, $2^3P_1$, $2^3P_2$, respectively.

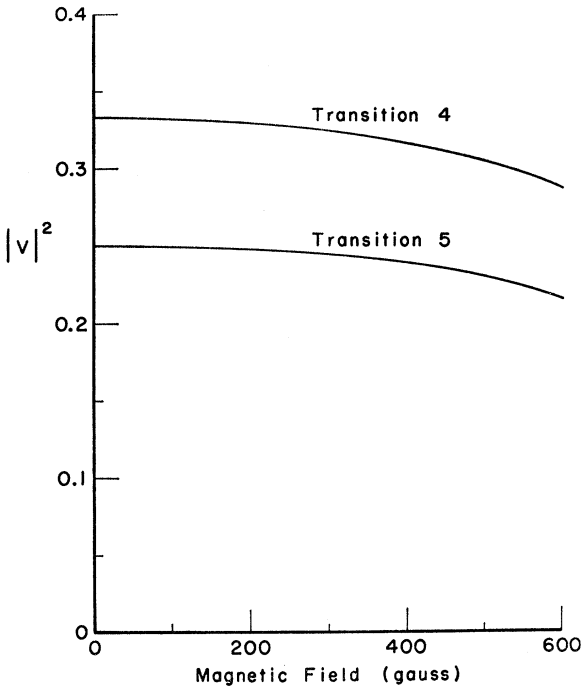


FIG. 7. Magnetic-field variation of $|V|^2$ for transitions 4 and 5. $V$ is the oscillatory field matrix element defined in Eq. (22).

the terms with $(E_1-E_2)^{-1}$ in Eq. (17) will be much larger than those with $(E_0-E_1)^{-1}$. It will be seen that $S(0\rightarrow+1)$ for transition 4 increases as a function of field, while $S(0\rightarrow-1)$ decreases. Figure 3 shows a field-dependent plot of (a) the $2^3P_1$ and $^3P_2$ energy levels (the arrows joining the relevant sublevels define transitions 4 and 5; the energies are given in MHz), (b) the frequencies of transitions 4 and 5, and (c) the relative signal strengths of transitions 4 and 5 for $\rho(\alpha,\beta)=0.5$. One notices that transition 5 is not observable at zero field. The natural linewidth of the transitions, determined by the radiative lifetime of the $2^3P$ state, is about 3 MHz, and at fairly low fields transitions 4 and 5 are not resolved.

### D. Line Shapes

Transitions between the optically excited $2^3P$ sublevels were induced by the presence of an oscillating electromagnetic field. The mechanism is a magnetic-dipole contribution to the Hamiltonian:

$$\mathcal{H}_{rf}=g_s\mu_0\mathbf{S}\cdot\mathbf{H}_1+g_L\mu_0\mathbf{L}\cdot\mathbf{H}_1, \quad (18)$$

where $\mathbf{H}_1$ is the magnetic component of the oscillatory field:

$$\mathbf{H}_1=2\mathbf{h}_1H_1\cos\omega t. \quad (19)$$

$\mathbf{h}_1$ is a unit polarization vector, $2H_1$ the amplitude of the oscillatory magnetic field, and $\omega$ the angular frequency of oscillation.

We consider an isolated pair of $2^3P$ sublevels, and assume the time-dependent wave function to have the

form

$$\Psi(\mathcal{J},m,\mathcal{J}',m',t)=a(t)\Psi(\mathcal{J},m)+b(t)\Psi(\mathcal{J}'m'). \quad (20)$$

$a(t)$, $b(t)$ are time-dependent probability amplitudes, and $\Psi(\mathcal{J},m)$, $\Psi(\mathcal{J}'m')$ are the time-independent eigenfunctions [Eq. (4)] of the relevant pair of $2^3P$ sublevels.

The time-dependent Schrödinger equation can be written

$$\begin{aligned} i\dot{a}(t)&=\mu_0H_1Ve^{i(\omega-\omega_{\alpha\beta})t}b(t)-\tfrac{1}{2}i\gamma a(t),\\ i\dot{b}(t)&=\mu_0H_1V^*e^{i(\omega_{\alpha\beta}-\omega)t}a(t)-\tfrac{1}{2}i\gamma b(t). \end{aligned} \quad (21)$$

$\omega_{\alpha\beta}$ is the energy separation, in angular frequency units, between the $2^3P$ sublevels $(\mathcal{J},m)$ and $(\mathcal{J}'m')$, i.e., the resonant transition frequency. $\gamma$ is the rate for radiative decay of the $2^3P$ state. It is assumed that $\gamma$ has the same value for all $2^3P$ sublevels. $V$ is the time-independent part of the matrix element representing the coupling between $(\mathcal{J},m)$ and $(\mathcal{J}',m')$ due to the oscillatory field:

$$V=\langle\Psi(\mathcal{J}'m')|(g_L\mathbf{L}+g_s\mathbf{S})\cdot\mathbf{h}_1|\Psi(\mathcal{J},m)\rangle. \quad (22)$$

These elements have been calculated by Lamb,[15] and are obtained using Eq. (5). Figure 7 shows the variation of $|V|^2$ as a function of magnetic field for transitions 4 and 5. It can be seen that for the fields of interest (up to 500 G), $|V|^2$ does not change appreciably for either transition, and therefore contributes little to the field-dependent signal variations discussed above. The cases of transitions 4 and 5 have $m=m'$ in Eq. (22), and the matrix element vanishes unless $\mathbf{h}_1$ is in the $z$ direction (i.e., parallel to the static magnetic field).

Equations (21) have assumed that the oscillatory field has been resolved into rotating components, and only the component near resonances has been included in each of the two equations. The (Bloch-Siegert) correction[18] for the other component will be discussed in Sec. V A 4.

Consider an atom excited to state $(\mathcal{J},m)$ at time $t=0$. This requires the initial conditions $a(0)=1$, $b(0)=0$. The resultant solutions to Eqs. (21) at time $t$ are

$$|b(t)|^2=\frac{4(\mu_0H_1)^2|V|^2\sin^2\tfrac{1}{2}[(\omega_{\alpha\beta}-\omega)^2+4(\mu_0H_1)^2|V|^2]^{1/2}t}{(\omega_{\alpha\beta}-\omega)^2+4(\mu_0H_1)^2|V|^2}e^{-\gamma t}=1-|a(t)|^2. \quad (23)$$

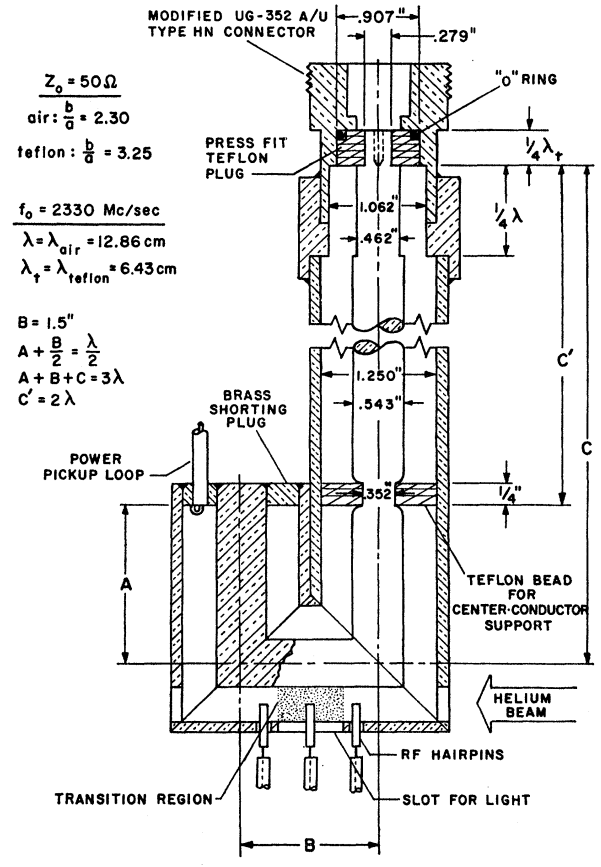


FIG. 8. The microwave transmission line (loop) viewed in cross section. a and b are, respectively, the radii of the inner and outer conductors.

The probability that the atom will decay during a time interval $dt$ after time $t$ is $\gamma e^{-\gamma t}dt$. This atom contributes to a signal in our experiment if it decays from state $(\mathcal{J}'m')$, the probability for which is the Lorentzian

$$\gamma\int_0^\infty|b(t)|^2dt=\frac{2(\mu_0H_1)^2|V|^2}{(\omega_{\alpha\beta}-\omega)^2+4(\mu_0H_1)^2|V|^2+\gamma^2}=\rho(\alpha,\beta). \quad (24)$$

Equation (24) should be substituted for $\rho(\alpha,\beta)$ in Eq. (12), and gives the expected line shape for the resonant transition signal if a plot is made by varying $\omega$ or $\omega_{\alpha\beta}$. In the present experiment, $\omega_{\alpha\beta}$, the resonant frequency, was varied by sweeping the static magnetic field. The "natural" linewidth, in the limit of vanishing $H_1$, is given by $2\gamma$, where the decay rate $\gamma$ is about $10^7$ per sec.[19] The natural linewidth in frequency units is

$$\Delta\nu=2\gamma/2\pi \text{ Hz}\sim3.2 \text{ MHz}. \quad (25)$$

The optimum amount of power broadening is obtained when the ratio of height to width is a maximum. This situation exists when the linewidth is broadened to $\sqrt{2}\gamma/\pi$, and the required amplitude of the oscillatory field is

$$2H_1=\sqrt{2}\gamma/\mu_0|V|\sim3 \text{ G} \quad \text{for transition 4}. \quad (26)$$

The units of $\mu_0$ are rad $\text{sec}^{-1}$ $\text{G}^{-1}$.

[18] F. Bloch and A. Siegert, Phys. Rev. **57**, 552 (1940); Jon H. Shirley, *ibid.* **138**, B979 (1965).

[19] W. R. Bennett, Jr., P. J. Kindlmann, and G. N. Mercer, Appl. Opt. Suppl. **2**, 34 (1965).

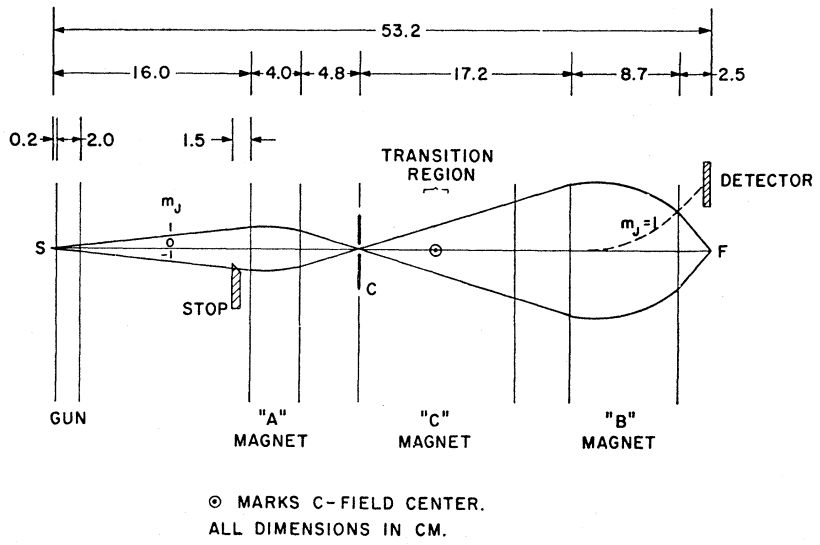


FIG. 9. An illustration of the $2^3S_1(m_S)$ trajectories. The vertical scale has been exaggerated by a factor of about 500. The trajectory of an atom which has undergone a transition $m_S=0\rightarrow+1$ is shown by the broken line striking an off-axis detector.

The oscillatory field in our experiment was obtained by allowing the atoms to pass along a coaxial microwave transmission line (Fig. 8). The amplitude in the $z$ direction, as seen by a given atom, was proportional to its radial distance from the axis of the transmission line. The true line shape was obtained by integrating Eq. (24) over the relevant part of the transmission-line cross section, giving for the signal

$$\rho(\alpha,\beta)=\frac{A}{C^{1/2}}\arctan\left\{\frac{1\cdot3(C/B)^{1/2}}{1+2\cdot3(C/B)^{1/2}}\right\}, \qquad (27)$$

where $A$ is an arbitrary normalization constant; $B/r^2=4[\mu_0H_1(r)]^2|V|^2$, $r$ being the radial distance from the axis of the transmission line, and $C=(\omega-\omega_{\alpha\beta})^2+\gamma^2$. The derivation of Eq. (27) has assumed a ratio of 2.3 to 1, respectively, for the radii of the outer and inner conductors (50-Ω impedance). This line shape differed little from a simple Lorentzian.

The derivation of Eqs. (12) and (24) was based on a simple model of the optical-microwave double-resonance process. The analysis of signal strengths and line shapes was an important factor in our data reduction, and it was necessary to examine the implications of a more rigorous mathematical model. A detailed formulation of the time-dependent Schrödinger equation leads to a set of coupled differential equations which have the same form as (21), but include the optical radiation field, and thereby introduce the time-dependent amplitudes of all the "ground" and excited substates coupled by this field. The solutions of such a set of equations have been considered previously in studies of excited states of hydrogen,[20] and of the phenomena of resonance trapping,[21] light shifts,[22] and light "beats"[23] in optical pumping. A calculation applied specifically to the conditions of an experiment such as the present, is contained in an unpublished report by Serber[24] (see Appendix B). His analysis and results are very similar to those of Barrat and Cohen-Tannoudji,[22] although they differ somewhat in details of formulation. The results indicate that Eqs. (12) and (24) are indeed valid if one includes small shifts in the expression for the resonant frequency $\omega_{\alpha\beta}$. These shifts arise from (a) the applied optical radiation (light shift) and (b) nonresonant components of the applied microwave field (Bloch-Siegert shift).[18] The latter is treated in Sec. V A 4.

The apparent shifts of energy levels in the presence of optical radiation arise from two distinct mechanisms. The first is due to a transfer of "coherence" between ground and excited states. (In this context the term "coherence" refers to the phase relationships between the Larmor precessions in the two sets of states.) This mechanism would apply to shifts in the excited states only under a set of special conditions which did not exist in our experiment.

The second type of light shift can be interpreted in terms of virtual transitions, due to photons whose energies are not exactly resonant with the ground-state–excited-state separations. We have estimated that in our experiment this effect would lead to shifts of less than 100 Hz in the $2^3P$ levels, and these are entirely negligible.

Light shifts in the $2^3S$ state of helium have been observed experimentally by Schearer.[25]

[20] W. E. Lamb, Jr., and T. M. Sanders, Phys. Rev. **119**, 1901 (1960); L. R. Wilcox and W. E. Lamb, Jr., *ibid.* **119**, 1915 (1960).
[21] J. P. Barrat, J. Phys. Radium **20**, 541 (1959); **20**, 633 (1959); **20**, 657 (1959).
[22] J. P. Barrat and C. Cohen-Tannoudji, J. Phys. Radium **22**, 329 (1961); **22**, 443 (1961); C. Cohen-Tannoudji, Ann. Phys. (Paris) **7**, 423 (1962).
[23] J. N. Dodd and G. W. Series, Proc. Roy. Soc. (London) **A263**, 353 (1961); J. P. Barrat, *ibid.* **A263**, 371 (1961).
[24] R. Serber, Columbia Radiation Laboratory Special Technical Report, 1965 (unpublished).
[25] L. D. Schearer, Phys. Rev. **127**, 512 (1961).

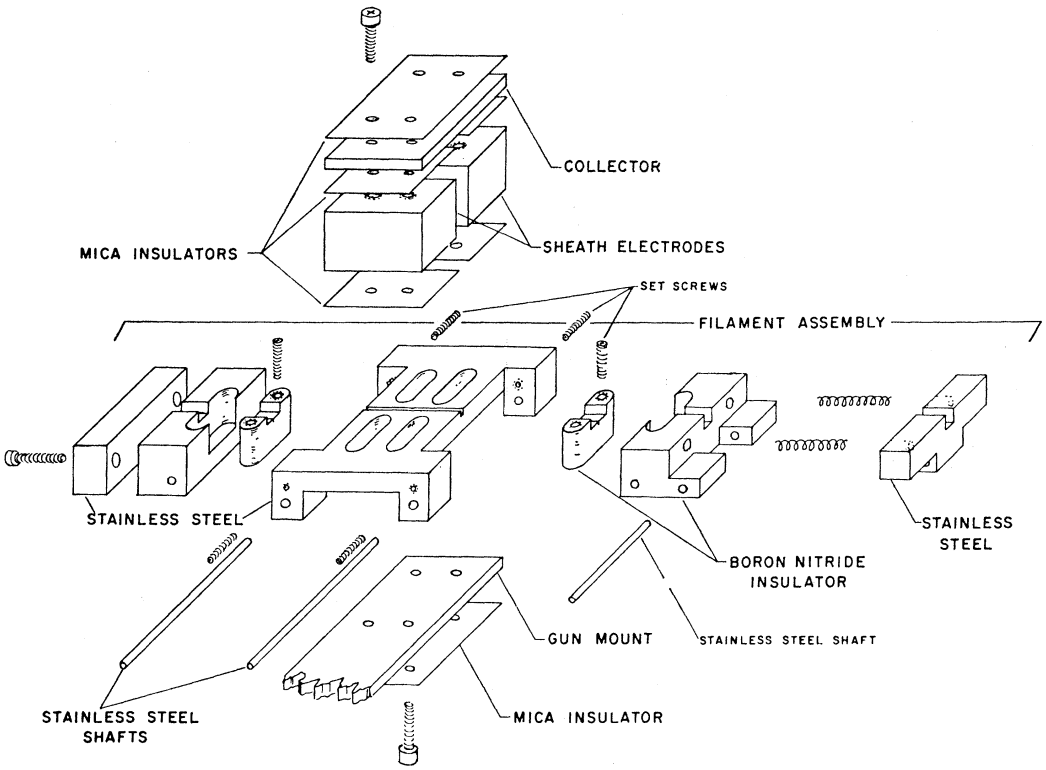


FIG. 10. Exploded assembly diagram of the electron gun.

## III. APPARATUS

A conventional atomic-beam magnetic-resonance apparatus (Fig. 4), with two deflecting magnets A, B, was used to separate the $2^3S(m_S)$ sublevels into different trajectories. The apparatus used had oppositely directed $A$- and $B$-field gradients which, together with a collimator, defined the $m_S=+1$, 0, $-1$ trajectories reaching the detector, as shown in Fig. 9. Between the A and B magnets was a uniform magnetic-field region C wherein transitions were induced between the $m_S$ substates. When such transitions occur, the atomic trajectories are altered, and the atoms involved no longer reach the detector. In our case it was desirable to observe transitions between specific substates, and this was accomplished by placing an obstacle near the $A$ field, and by moving the detector to one side. In Fig. 9 we illustrate the obstacle-detector configuration for observation of the $m_J=0\rightarrow+1$ transition.

Transitions between the $m_J$ sublevels of the $^3S_1$ beam were effected by optically exciting the atoms to the $2^3P$ state, using a helium discharge lamp placed in the $C$-field region. Atoms in the $2^3P$ state decay only to the $2^3S$ state, since optical transitions to the $1^1S_0$ ground state are doubly forbidden. The radiative lifetime of the $2^3P$ state is about $1\times10^{-7}$ sec, whereas the transit time for the atoms through the $C$ field was about $5\times10^{-5}$ sec.

The vacuum system and deflecting magnets were those used by Drake *et al.* in the measurement of the atomic moment of the $2^3S_1$ state of helium.[26] Selection of specific trajectories was somewhat sensitive to drifts in the $A$- and $B$-magnet currents, and these were carefully monitored during the course of a measurement.

In general the $2^3P$ resonance signals amounted to 10% or less of the number of atoms reaching the detector. Observation of these signals was enhanced by a scheme of synchronous detection. The microwave field inducing magnetic resonances between the $2^3P$ sublevels was on-off modulated by a low-frequency square wave. The modulation was synchronized with a channel switch in the detector system, so that the beam intensity was recorded separately for the microwave field on and off. This operation was equivalent to phase-sensitive detection, and, since digital techniques were used to count the atoms in the beam, integrating times of several minutes were attainable. The atom counts in the "off" channel provided continuous normalization of the signal, and hence the measured signal was virtually independent of fluctuations in the total beam intensity. The measured signal was not, however, independent of fluctuations in the intensities of either the microwave field or the exciting optical radiation, since these had a direct effect on the relative magnitude of the signal itself.

[26] C. W. Drake, V. W. Hughes, A. Lurio, and J. A. White, Phys. Rev. **112**, 1627 (1958); C. W. Drake, thesis, Yale University, 1958 (unpublished).

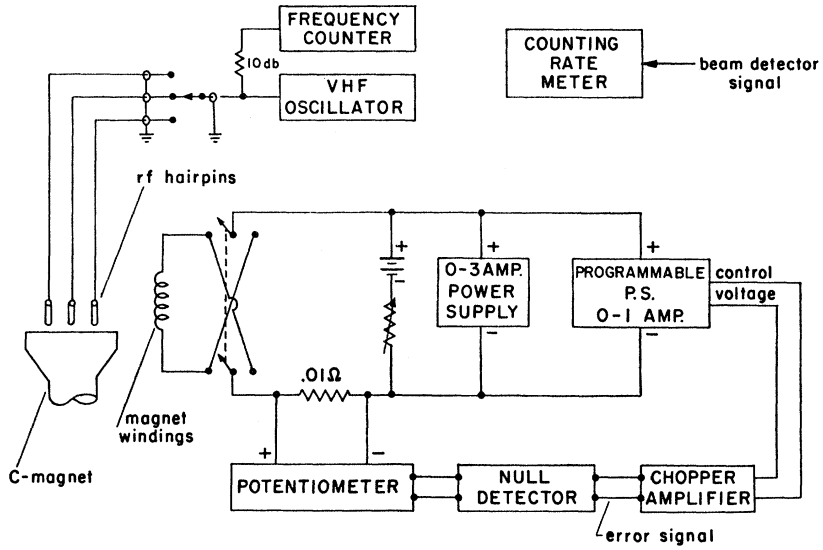


FIG. 11. Block diagram of the $C$ magnet power supply. The upper part of the diagram indicates how the $C$ field was measured by observing $2^3S_1$ Zeeman resonances in the atomic beam.

### A. Atomic Source

#### *1. Gas-Handling System*

Commercial-grade helium was stored in a reservoir at a pressure of about 1 atm. The gas was allowed to diffuse into the vacuum system through a slit situated at the entrance to the electron gun. The dimensions of the slit were 0.625 by 0.006 in. Helium flowing from the reservoir was controlled by a needle valve. The helium pressure prior to diffusion through the slit was estimated to be about 0.1 mm Hg.

#### *2. Electron Gun*

Electron bombardment was used to excite the ground-state atoms into the metastable $^3S_1$ state. The electron gun, shown exploded in Fig. 10, is of the "sheath electrode" design, similar to that used by Lamb and Retherford.[27] The filament was a piece of 2% thoriated tungsten wire, 2 in. long and 0.006 in. in diameter. A moderate amount of spring tension was applied to keep it straight. The electrons emitted were accelerated into the U-shaped anode gap, where they crossed the helium beam. Longitudinal focussing of the electron beam was obtained by placing the gun within the poles of a permanent magnet. The focussing field was approximately 1000 G. The collector and side-electrode portions of the anode were at the same potential, but the electron current to the collector could be measured separately. The relative positions of the electron gun and the focussing magnet could be adjusted to maximize the fraction of the emission current reaching the collector. The emission current was normally 20 to 30 mA with about 80% of this reaching the collector. The filament required between 1.7 and 2.2 A of heater current, which was supplied at a frequency of about 7 kHz. At lower frequencies the filament tended to vibrate due to the presence of the magnetic field. The filament-cathode potential was maintained at 30 V, some 10 V about the $2^3S_1$ excitation threshold, because of space-charge effects within the anode sheath. Several different techniques were tried in activating the filament. The method that gave the best results was to increase gradually the heater current from about 1.2 A to a maximum of 2.4 A, the rate of increase being about 0.2 A/h. It was believed that the presence of hydrocarbons from the diffusion-pump oil played an important role in the activation process.[28]

### B. *C* Magnet

The $C$ magnet was originally used by White *et al.*[29] in the measurement of the hyperfine structure of the $2^3S_1$ state of $He^3$. The circular pole faces were 5 in. in diameter and were separated by a gap of 1.6 in. The magnetizing current was obtained from a 4-V lead battery, and fields up to 1000 G were attainable with currents in the region of 100 A.

The circuitry associated with the $C$ field is shown in Fig. 11. A variable resistor in series with the battery was used to make large adjustments to the current. Fine adjustment was accomplished by means of a 0–3-A electronic power supply in parallel with the battery-resistor combination.

A current stabilizer was used to reduce drifts in the magnetic field while data were being taken. The voltage drop across a 0.01-Ω resistor was measured with a potentiometer. The deviation of this voltage from a preset value was amplified, and fed as an error signal to the controls of a programmable 0–1-A power supply. This

[27] W. E. Lamb, Jr., and R. C. Retherford, Phys. Rev. 81, 222 (1951).

[28] P. Schneider, J. Chem. Phys. 28, 675 (1958).

[29] J. A. White, L. Y. Chow, C. W. Drake, and V. W. Hughes, Phys. Rev. Letters 3, 428 (1959); J. A. White, thesis, Yale University, 1958 (unpublished).

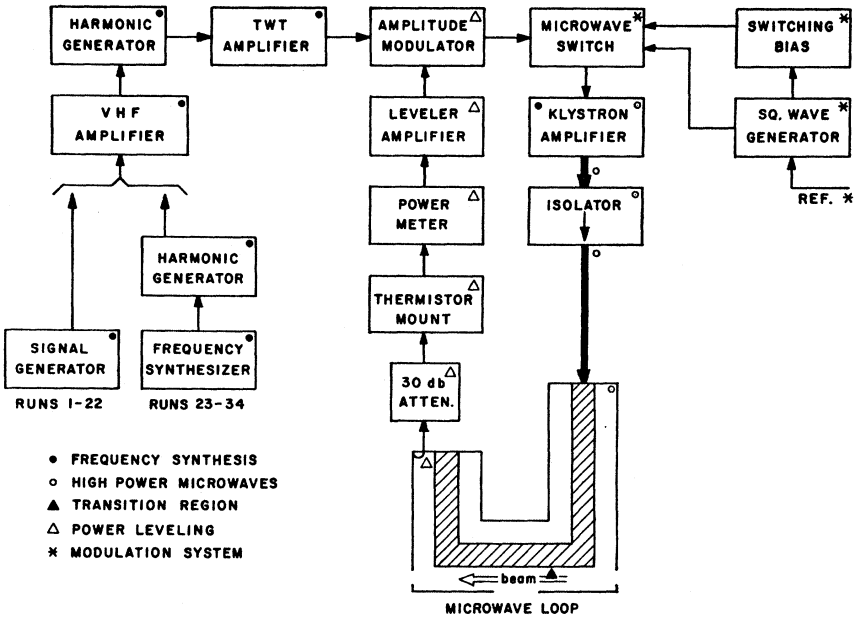


FIG. 12. Block diagram of the microwave system. The purpose of each component is indicated by the appropriate symbol, keyed in the bottom left-hand corner of the diagram.

power supply, which was in parallel with the battery, provided a correction current to compensate for any drifts in the magnet current. The over-all gain of this feedback loop was about 10, and this was sufficient to reduce current drifts to less than 1 part in $10^4$ per hour.

A set of current shims was placed on the pole faces of the magnet. These consisted of a series of coils made of No. 30 gauge varnished copper wire embedded in Teflon sheet 0.125 in. thick. The shapes and dimensons of the coils were designed to remove linear and quadratic field gradients along the axis of the atomic beam.[30]

The field was measured by inducing Zeeman resonances in the $2^3S_1$ beam. The frequencies of these transitions had a linear field dependence which was very accurately known.[26] Three separate rf loops were used to induce the Zeeman transitions (see Fig. 8), and the resonance frequencies at all three were measured for a given field setting. In this way the average field in the optical excitation region could be measured with an accuracy of 3 parts in $10^5$ or better.

### C. Light Source

A commercial helium discharge lamp[31] was used to excite optically the $2^3P$ states. It consisted of a small quartz Geissler tube, mounted in a Pyrex jacket filled with nitrogen to a pressure of 100 Torr. The lamp was placed inside the vacuum system underneath the gap of the $C$ field. The Pyrex outer jacket was wrapped in aluminum foil and then pushed into a tight-fitting brass sleeve. A light pipe 2.5 in. long was placed over a 0.75-in.-diam aperture in the sleeve. When the lamp was initially placed in the sleeve, care was taken to ensure that the brightest part of the discharge was in line with the aperture. The main purpose of the light pipe was to shield the atoms outside the $C$ region from the radiation. The intensity of the emitted radiation appeared to be adequately stable for our purpose; when in the apparatus, however, it was subject to the fringing field of the $C$ magnet, and there were noticeable variations in intensity when the field was changed by large amounts. These variations are not believed to have affected the precision of our experiment.

A typical emission spectrum of the $2^3S_1 \rightarrow 2^3P_J$ transitions has been shown in Fig. 6. The relevance of the spectral distribution to the calculations of signal intensities has been discussed in Sec. II.

### D. Microwave System

A block diagram of the system is shown in Fig. 12. The microwave field intensity required to induce magnetic-resonance transitions within the $2^3P$ state was provided by a 1-kW klystron amplifier. The frequency of the input to the klystron was the preamplified 60th harmonic of a crystal-controlled oscillator. This input was square-wave modulated in synchronism with the channel switching of the detector system. A second modulator in the input line served to keep the power level constant. It was controlled by a voltage which varied with the amplitude of the microwave field in the $C$ region.

#### *1. Frequency Synthesizer*

The crystal-controlled oscillator used initially was a Gertsch FM-6 frequency synthesizer. The output of the FM-6 was rich in harmonics, and one of these harmonics at about 250 MHz was fed into a tuned very-high-

[30] W. A. Anderson, Rev. Sci. Instr. 32, 241 (1961).
[31] Philips type 93098E.

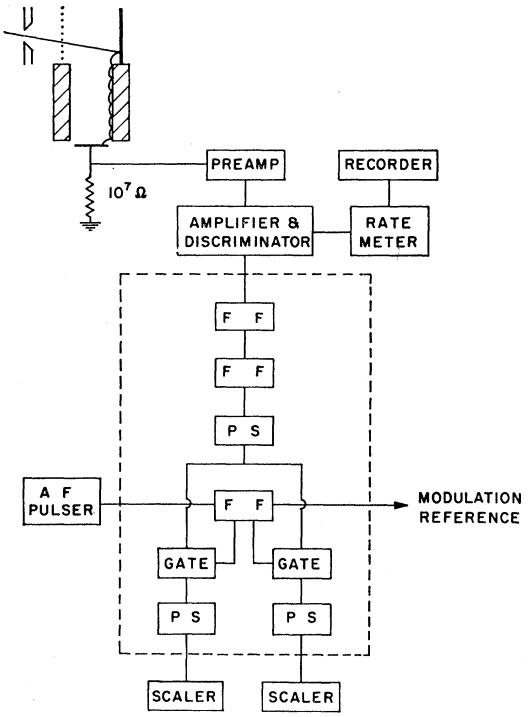


FIG. 13. Block diagram of the detection system. FF and PS represent flip-flop and pulse-shaping modules, respectively. The detector slit and electron multiplier are illustrated in the upper left-hand corner.

frequency (VHF) amplifier. The required frequency in the range 2295 to 2420 MHz was obtained by generating harmonics using a step recovery diode at the output of the VHF amplifier. This harmonic was amplified to a level of 2 or 3 mW using a travelling-wave tube amplifier. The square-wave modulation was accomplished using a commercial diode switch, which was operated by an audio square-wave generator, and this in turn was triggered by the detector channel switching circuit described below.

The Gertsch frequency synthesizer was, for our purpose, superseded by a Hewlett-Packard 0–50-MHz frequency synthesizer. This was more convenient than the Gertsch because it was more stable and its frequency could be varied in finer steps. A crystal diode, in series with this synthesizer, was used to generate harmonics in the VHF region.

### 2. *High-Power Microwaves*

A Varian VA-802B klystron amplifier was used to generate the 500–1000 W of power needed to induce the $^3P$ transitions. This klystron was a four-stage tuned amplifier and had a power gain of about $10^6$. After about 10 000 h of operation the klystron was still delivering about 600 W with a power gain of $10^5$. The output of the klystron went to a ferrite isolator, and then to the atomic-beam apparatus via a flexible coaxial cable. The reflected power was dissipated in the isolator which was firmly bolted to a water-cooled plate. The type-*N* connectors on the isolator were air cooled.

### 3. *Microwave Transmission Line*

The interaction between the microwave field, optical radiation, and atomic beam took place within a shorted coaxial transmission line (Fig. 8), briefly referred to as the "loop." Microwave power entered the loop through a modified HN connector. The vacuum seal at the connector was effected by a cylindrical Teflon plug, which fitted very tightly around the inner conductor, and pressed an O ring against the outer conductor. The inner and outer conductors were made of brass, and the ratio of their diameters was such as to provide a 50-Ω characteristic impedance. All joints were silver-soldered. The length of the line was designed to provide an *H*-field maximum at the light-atom interaction region. The inner conductor was supported by a Teflon bead located at a suitable *E*-field minimum. A small pickup loop at the short was used to measure the the microwave-field intensity, and this controlled the power-levelling system.

The microwave-magnetic-field lines were a series of circles concentric with the inner and outer conductors of the coaxial line. The ribbon-shaped atomic beam was essentially along a radius of these circles. The direction of the microwave field, as seen by the atoms, was effectively parallel to the *C* field, and therefore this setup was a suitable one for observing $\Delta m_J=0$ transitions. The intensity of the microwave field varied inversely as the radial distance from the center conductor, and this had to be averaged over the beam height. The effect of this nonuniformity in the microwave field on the resonance line shapes is discussed in Secs. II and V. The variation of the microwave-field intensity along the beam axis was negligible.

The atomic beam entered and left the loop through $\frac{1}{16}\times\frac{3}{8}$-in. slots in the elbows, and the optical radiation entered through a similar slot in the lower surface. The portion of the atomic beam crossed by the optical radiation defined the spectroscopy region. It was spanned by three rf "hairpins" which were used to excite Zeeman transitions in the $2^3S$ beam when the field was being measured.

### 4. *Power Leveling*

The intensity of the microwave magnetic field within the transmission line was monitored by means of the small loop, mentioned above, inserted at the shorted end. The output of this loop was rectified by a crystal detector, and then used as a feedback signal to control a PIN-diode modulator which was in series with the input to the power amplifier. This automatically adjusted the input to the power amplifier, and the field intensity within the transmission line was maintained

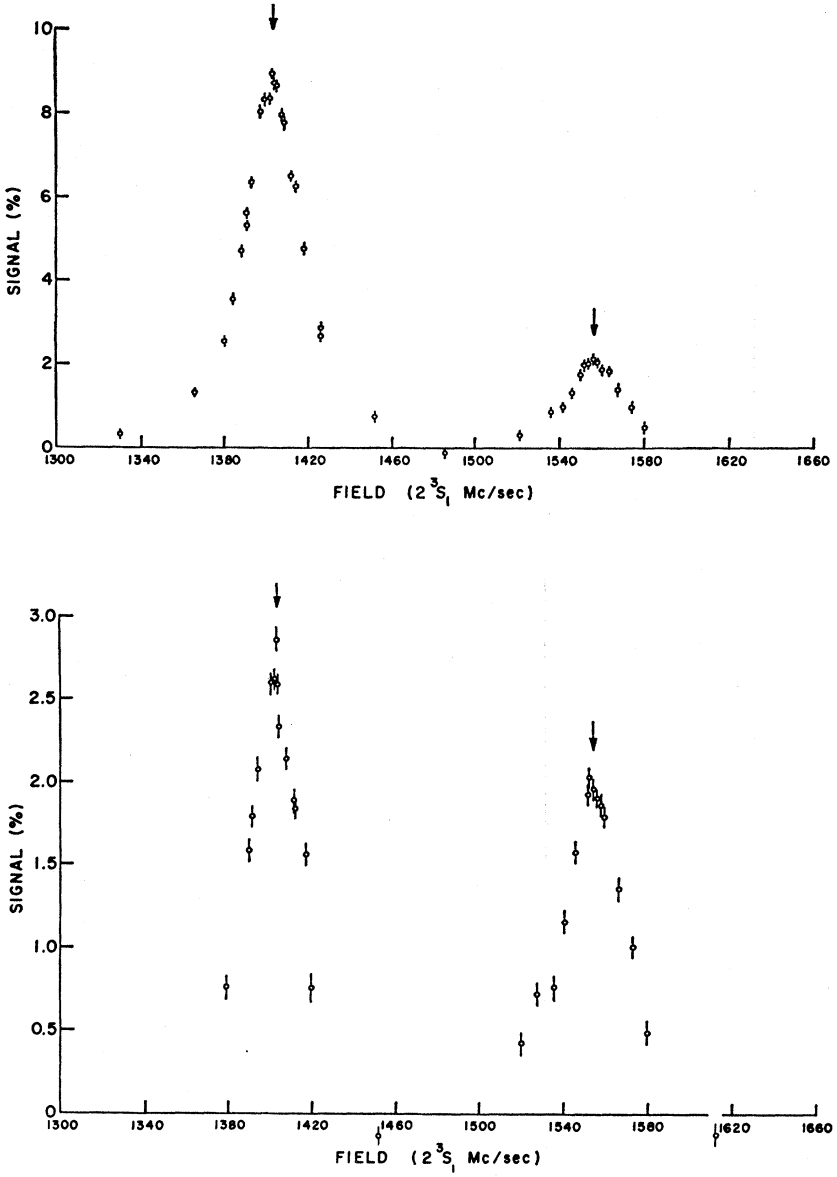


FIG. 14. Experimental plots of transitions 4 and 5 for a $2^3S(m_S)$ $(0 \rightarrow +1)$ trajectory. The plots were made by sweeping the magnetic field for a constant microwave frequency of 2420.0 MHz. The field, plotted in terms of the measured $2^3S_1$ Zeeman frequency (2.8 MHz per G), was in the region of 500 G. Transition 4 occurs at fields lower than transition 5.

constant to within about 2%. In addition, the power flowing through the transmission line was sampled by means of an attenuating decoupler and measured in a thermistor circuit.

### E. Detector System

The detection system is shown schematically in Fig. 13. The detector itself was defined by a slit. Metastable atoms passing through the slit impinged on the cathode of an electron multiplier, releasing Auger[32] electrons. The amplified electron pulses were gated alternately into "microwaves-on" and "microwaves-off" channels. The signal due to a $2^3P$ magnetic resonance was therefore proportional to the excess counts in one channel.

#### *1. Metastable Atom Detection*

The electron multiplier (top left corner of Fig. 13) was of the crossed-field, continuous dynode variety, with a tungsten cathode.[33] The Auger ejection efficiency for helium $2^3S$ metastable atoms from a tungsten surface is about 40%.[32] The fraction of Auger electrons at the multiplier cathode which gave measurable pulses at the anode was not known precisely, but it was estimated that 10% of the metastable atoms reaching the detector gave measurable pulses.

The multiplier pulses, after amplification, triggered a discriminator, which was used to suppress low-level

[32] R. Dorrenstein, Physica **9**, 447 (1942); G. J. Schulz and R. E. Fox, Phys. Rev. **106**, 1179 (1957); H. D. Hagstrum, *ibid.* **96**, 336 (1954).

[33] Bendix type M306.

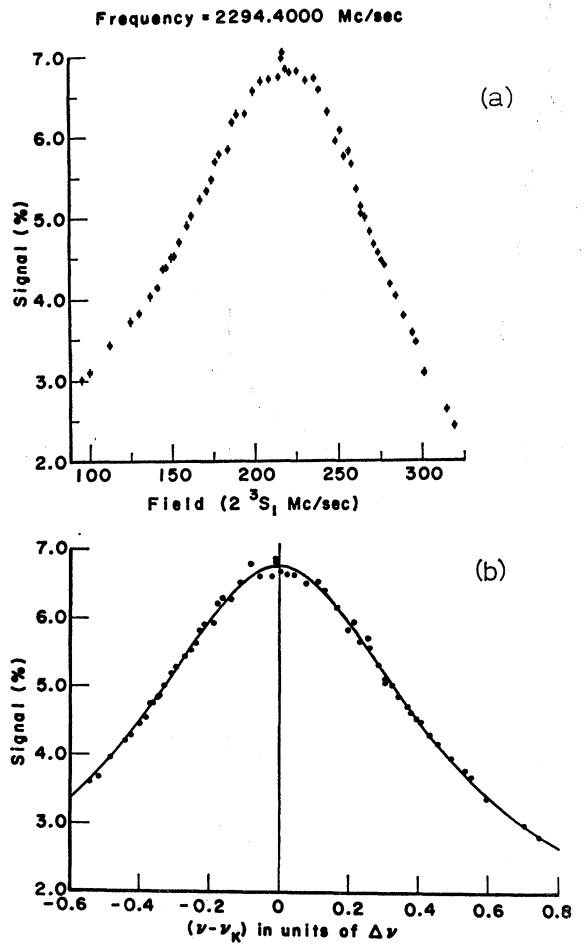


FIG. 15. (a) Experimental plot of a low-field transition-4 resonance. The magnetic field, measured in terms of the $2^3S_1$ Zeeman resonance frequency (2.8 MHz per G), was swept for a constant microwave frequency of 2294.4000 MHz. (b) Least-squares fit of the plot, Fig. 15(a), to the theoretical line shape, Eq. (27). The field points have been converted into transition-4 frequency units, and plotted as a fraction of the linewidth $\Delta\nu$.

pulses largely due to noise. Pulses passing the discriminator were then processed by a logic network directing them into the proper channel. A second output from the amplifier was recorded on a pulse-rate meter. This was used to monitor the beam intensity, and to observe $2^3S$ Zeeman resonances when measuring the $C$ field.

### 2. *Modulation Logic*

Gating was achieved by means of a network of flip-flop, pulse shaping, and gate modules as shown in Fig. 14. Rise-times in the logic circuitry were typically 20 nsec. In addition, two flip-flops were used to scale down the input pulse rate by a factor of 4 to avoid overloading the scalers. These pulses were then applied simultaneously to two gate modules, which were opened alternately, for equal time intervals, in phase with the microwave modulation. The gates were activated by conjugate outputs of a flip-flop module, which was triggered by a pulse generator running at 100 pulses/sec. The flip-flop output was therefore a symmetric 50-Hz square wave. A third output from the flip-flop was used to activate the microwave switch, thereby synchronizing the microwave modulation with the channel switching.

This gating system was carefully checked for instrumental asymmetries.

## IV. EXPERIMENTAL PROCEDURE

The computed relative intensities of transitions 4 and 5 were verified experimentally as illustrated in Fig. 14. The plots were made by sweeping the magnetic field. It can be seen that the relative intensities differ as expected for the $2^3S(m_S)$ trajectories $(0\rightarrow+1)$ and $(0\rightarrow-1)$. The relative intensities were not precisely as predicted because the transition-5 signal was affected slightly by imperfect state selection in the beam geometry. In addition, the transition-4 intensities differed somewhat from those calculated because the polarization of the exciting radiation was not uniformly distributed in the $xz$ plane. The absolute values of the signals were somewhat less than calculated due to incomplete separation of the trajectories. There was a substantial background from the tail of the central beam which was much larger than the $(0\rightarrow\pm1)$ trajectories. This meant that some of the detected atoms had not been optically excited. The amount of background could be measured from the change in off-axis beam intensity when switching on the optical radiation. In general, about half the detected atoms had been optically excited.

Two typical experimental plots of transition-4 resonances are shown in Figs. 15(a) and 16(a). Each point on the plot consists of a reading of the $2^3P$ signal for a fixed value of the magnetic field. The field value was obtained from the frequency of the Zeeman resonance in the $2^3S$ beam. It was not possible to measure the field and observe the $2^3P$ signal simultaneously. Field measurements were made both before and after a transition-4 reading. Approximately 15 min were required to register adequate counts for the $2^3P$ resonance, and the drift in field during this period was kept below 100 ppm by the $C$-magnet current regulator. The smallness of this drift, coupled with the fact that transition 4 was relatively field-independent, meant that the assumption of a field drift linear with time was adequate, and an average was made of the field measurements before and after the recording of the $2^3P$ signal.

The uniformity of the $C$ field was estimated by making separate $2^3S$ resonance measurements at each of the rf loops spanning the optical microwave region (Fig. 8), and then corrective adjustments were made on the shim coils. The field measurement itself was an average taken over the three points in the optical microwave region. This spatial average was based on

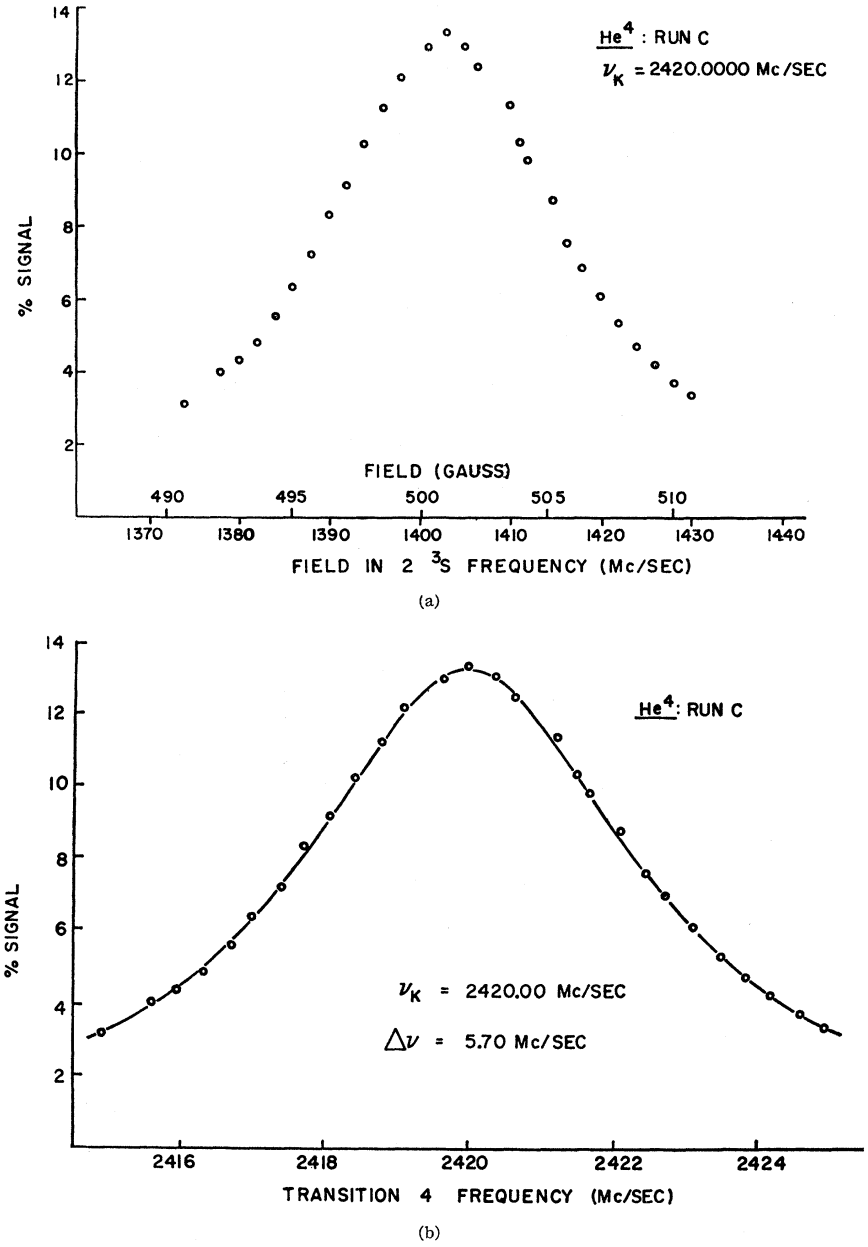


FIG. 16. (a) Experimental plot of a high-field transition-4 resonance. The magnetic field was swept for a constant microwave frequency of 2420.0000 MHz. (b) Least-squares fit of the plot, Fig. 16(a), to the theoretical line shape, Eq. (27). The field points have been converted into transition-4 frequency units.

the assumption that the magnitude of field as a function of distance along the beam axis could be approximated by a parabola. The use of shim coils and the spatial averaging technique resulted in an accuracy of perhaps 10 ppm in the measurement of the average field. The field inhomogeneity over the region of interest was usually less than one in $10^4$.

The $^3P$ transition 4 signal was recorded by allowing the microwaves-off scaler to run to a preset value (usually $10^7$ counts). The signal intensity was then evaluated as the difference between the microwaves-on and microwaves-off counts expressed as a fraction of the latter. The peak signals ranged between $4\times10^5$ and $12\times10^5$ counts, and the statistical uncertainty was about $5\times10^3$ counts. The two scalers were started and stopped simultaneously and at random with respect to the phase of the modulation. The resultant switching error due to one-channel counting for up to one modulation semicycle more than the other could never have exceeded 250 counts. Flip-flop logic ensured that the on period for each channel was a modulation semicycle, to an accuracy of about 1 $\mu$ sec (or about one in $10^4$). The square-wave symmetry of the microwave modulation, however, was accurate only to about 1%, because synchronism with the channel-switching was effected only at the onset of each full modulation cycle. This

resulted in a small reduction in signal, since either some signal was carried over into the off channel, or else the microwaves were off during a fraction of the on counting period. A similar effect arose from the fact that the modulated signal lagged the switching cycle in phase by about 0.5% of the modulation period, owing to the finite time taken by atoms in the optical microwave region to reach the detector. The reduction in signal by these two effects, at most about 5%, did not have any appreciable effect on the experimental precision, since there was no resultant distortion in the line shape.

The plotting of a complete line shape took several hours and it was vital that any parameters critically affecting the signal intensity remained stable throughout this period. The three important parameters in this respect were the following.

(a) Microwave field intensity: The power leveling system was subject to small drifts of about 1%, particularly in the crystal detector.

(b) Lamp intensity: Several hours were allowed for the lamp to reach thermal equilibrium in the vacuum system. It was our experience that the lamp intensity drifted by at most 1% during the course of our experiment. This was checked by periodically measuring the light flop, i.e., the total number of $2^3S$ atoms reoriented because of the effects of optical excitation and decay.

(c) Beam geometry: It was pointed out that the background when observing atoms in a $2^3S$ ($m_S=0\rightarrow\pm1$) trajectory was fairly sensitive to the location of both the $A$-field obstacle and the detector. Care was taken to locate these in the least critical positions, even at a sacrifice in signal intensity. The beam background became sensitive to scattering at pressures above $1\times10^{-6}$ Torr, and experiments were run only when the vacuum was substantially better than this.

The effect of any small drift in signal intensity was, to a large extent, compensated by plotting the points in symmetric pairs about the line center. This procedure reduced the effects of these drifts on our precision to negligible proportions. The extent of any drift was checked periodically by remeasuring the peak intensity. The plot was discarded if there was an indication of drifts in signal greater than 2% per hour.

Figure 15(a) was plotted for a klystron frequency of 2295 MHz and the field at the resonance peak was about 100 G (see Fig. 3). In this low-field region the field dependence of the transition frequency was very nonlinear, resulting in the asymmetry of the resonance. The average field dependence was small, and a wide sweep in field was required to plot the line shape. It may be seen from Fig. 3 that the inherent signal strength changed appreciably over the range of field spanned by the resonance, and a correction of some 20 ppm in the data was required to compensate for the resultant asymmetry in the line shape. For convenience we shall refer to this as the "slope" correction. In addition the small contribution of transition 5 was not resolved, necessitating a correction of some 5 ppm.

The plot of Fig. 16(a) was made at high field (centered around 500 G with a klystron frequency of 2420 MHz). Here the field dependence was larger and more linear, giving an almost symmetric line shape swept over a relatively narrow range of field. This narrower sweep, coupled with the smaller variation of signal strength with field, meant that the slope correction was almost negligible. In addition, transition 5 was well resolved, as shown in Fig. 14. All precision runs at high fields were taken on the $2^3S(m_S=0\rightarrow+1)$ trajectory, since at these fields the signal from the $(0\rightarrow-1)$ trajectory was far smaller (Fig. 14). In general the statistical standard deviations were slightly lower than those at low fields, due to the increased signal strength. At high fields uncertainties associated with the field measurement and reduction of the Zeeman Hamiltonian became more important; there was a correction, estimated to be some 10 ppm, arising from relativistic[16] and motional[17] corrections to the Zeeman Hamiltonian.

## V. DATA REDUCTION

The data provided by a plotted resonance were computer programmed to yield a value of the $2^3P_1-2^3P_2$ fine structure. The program was subdivided into four sections, which will be discussed separately.

### A. Signal Corrections

#### *1. Slope Correction*

The observed signal had to be adjusted to compensate for the variation of excitation and decay probabilities over the range of field spanned by the resonance. The results of Sec. II were used to compute the variation of inherent signal intensity as a function of field, $dS/dH$. An assumption that $dS/dH$ was constant over the range of the resonance proved to be more than adequate for the required precision. The calculated value of $dS/dH$ was compared with experiment by comparing the intensities of resonances observed at various fields (see Sec. II), and it was found that the calculated $dS/dH$ was about 20% too small. This was verified by comparing the results for the fine structure given by the resonances plotted from the $2^3S(m_S=0\rightarrow+1)$ trajectory, with those obtained from the $2^3S(m_S=0\rightarrow-1)$ trajectory. The slope corrections for the two trajectories have opposite signs [Eq. (17) and Fig. 3]. Results for the fine structure without the slope correction were thus too low in the case of one trajectory, and too high in the other. A value of $dS/dH$ some 20% larger than calculated was needed to bring the two sets of results into agreement. This 20% discrepancy between the theoretical and observed values of $dS/dH$ corresponded to a 4-ppm change in the measured fine structure for the low-field resonances, but was much less than 1 ppm for the high-field resonances. The correction was

actually applied by normalizing the signal value of each point in the plot with respect to the signal at the center of the resonance, using the observed value of $dS/dH$.

A possible explanation for the discrepancy in $dS/dH$ is that the polarization of the exciting radiation was not as assumed in Sec. II. The lamp was situated in stray fields from the $C$ magnet, and this may have given rise to additional polarization in the $z$ direction, accounting for the larger $dS/dH$.

### 2. Transition-5 Correction

The relative magnitudes of the signal intensities for transitions 4 and 5 were calculated as a function of field. These were compared with experiment as indicated in Sec. IV, and it was found that the observed relative magnitude of the transition-5 signal was larger than that calculated by almost a factor of 2. A probable explanation of this discrepancy was imperfect selection of the $2^3S$ trajectories, since the intensity of the transition-5 signal was particularly sensitive to this. On this basis a hypothetical plot was made of the unresolved transition-5 resonance, and this was subtracted from the observed resonance. The center of the transition-5 resonance was known to an accuracy more than adequate for the purpose of making this small correction.

### 3. Relativistic and Motional Corrections to the Zeeman Hamiltonian

Various terms of order $\alpha^2\mu_0 H$ must be included in the Zeeman Hamiltonian to account for relativistic effects.[16] The magnitudes of these terms have been estimated using a hydrogenic approximation for the radial wave function of the $1s2p$ configuration in helium. We plan to make high-precision measurements of the Zeeman transitions in the $2^3P$ state, and the results should provide an excellent check on the accuracy of the calculated corrections.

The corrections were applied by evaluating the matrix elements of the relativistic terms in the $(J,m)$ scheme, and then calculating their contributions to the transition-4 frequency. This contribution to the transition frequency was then subtracted from the experimental fine structure, a valid procedure owing to the relative smallness of the correction.

A further contribution to the Zeeman Hamiltonian [Eq. (1)] arises from the motion of the nucleus.[17] Equation (1) has been written under the assumption of an infinitely massive nucleus, and the correction terms are of order $(m/M)\mu_0 H$, where $m$ and $M$ are masses of the electron and nucleus, respectively. The motional terms are all proportional to $L_z$, and hence they can be incorporated conveniently as a modification in the value of $g_L$. Once again a hydrogenic approximation was used for the radial wave function. Some details of these calculations are given in Appendix C.

The relativistic and motional corrections each resulted in corrections of about 8 ppm to the high-field results, and about 3 ppm to the low-field results. Calculation of the motional correction was straightforward and a nominal uncertainty of 0.5 ppm was associated with it. The relativistic corrections, however, involved some two-electron operators which could depend critically on subtle properties of the radial wave functions. We have for this reason assigned an uncertainty of 3 ppm until the corrections have been verified experimentally.

### 4. Bloch-Siegert Correction

The interaction of the atom with the nonresonant rotating component of the microwave field leads to an asymmetry in the experimental line shape.[18] This can be compensated by applying a correction $\delta\omega$ to the center frequency $\omega$ [see Eq. (24)].

The correction is given by

$$\delta\omega=(\mu_0 H_1)^2|V|^2/\omega.$$

A direct measurement of $H_1$ was not practical, but it could be related to the measured linewidth

$$\Delta\omega=2\{\gamma^2+4(\mu_0 H_1)^2|V|^2\}^{1/2}.$$

Hence

$$\delta\omega=\{(\Delta\omega)^2-4\gamma^2\}/16\omega.$$

This correction amounted to about 0.2 ppm, and hence was negligible.

## B. Conversion of Field Values to Equivalent Transition-4 Frequencies

The resonances were plotted by varying the magnetic field, i.e., the quantity $\omega_{\alpha\beta}$ in Eq. (24). The value of $\omega_{\alpha\beta}$ had to be computed for each field point, and then a comparison could be made of the experimental data with the line shape of Eq. (24).

The $^3P_1(m_J=0)-^3P_2(m_J=0)$ energy-level separation was computed for each measured value of the magnetic field. A substitution

$$(\mu_0 H)_i=\nu_i(2^3S)/g_J(2^3S) \quad \text{in frequency units} \quad (28)$$

was made in the expressions for $W(1,0)$ and $W(2,0)$ (Table II). $\nu_i(2^3S)$ was the measured $2^3S$ Zeeman frequency for the $i$th point in a $2^3P$ resonance plot. The value of the $g$ factor $g_J(2^3S)$ was assumed to be 2.00223.[26] The expressions for $W(1,0)$ and $W(2,0)$ were solved by iteration, using the initial substitutions $W(1,0)=E_1$ and $W(2,0)=E_2$, respectively. Approximate values of $E_1$, $E_2$, accurate to about 20 ppm, were required to initiate the iterative solutions. A subtraction of the final solutions yielded a value for the transition-4 frequency which would be resonant at the $i$th field point:

$$(\omega_{\alpha\beta}/2\pi)_i=\nu_i(2^3P)=W(1,0)-W(2,0)=(E_1-E_2)+f[\nu_i(2^3S)], \quad (29a)$$

where $f[\nu_i(2^3S)]$ is some function of the $2^3S$ Zeeman frequency. The quantity $f[\nu_i(2^3S)]$ was in the range 5–40 MHz for the low-field runs, and was about 130 MHz for the high-field runs.

### C. Least-Squares Fit of Theoretical Line Shape

Both the Lorentzian [Eq. (24)] and the true [Eq. (27)] line shapes were fitted to the experimental resonances. This enabled us to estimate the extent to which an error in averaging the microwave-field distribution might have affected the precision of the fine-structure determination. The two line shapes were, in fact, almost identical, both being symmetric about their peaks when plotted as functions of $\nu_i(2^3P)$. The results for the fine structure in the two cases differed by less than 1 ppm, and we concluded that any errors in averaging the microwave field were effectively negligible. The true line shape gave slightly more weight to points plotted in the tails of the resonance, and the small difference in results arose when points were plotted further out in the tail on one side of the resonance than on the other.

Comparison with experiment was achieved by rewriting Eq. (24) in the form

$$S_i=\frac{D}{[\nu_i(2^3P)-\nu_c]^2+(\frac{1}{2}\nu_{1/2})^2}. \tag{24'}$$

Here, $S_i$ is the signal and $D$ is a constant normalizing the peak signal to that observed experimentally. $\nu_{1/2}$ is the experimental linewidth, and $\nu_c$ the value of $\nu_i(2^3P)$ at the center of the resonance:

$$\nu_c=E_1-E_2+f[\nu_c(2^3S)]. \tag{29b}$$

$D$, $\nu_{1/2}$, and $\nu_c$ were the parameters to be determined by fitting the experimental points to the analytic line shape. The value of $\nu_c$ thus determined was equated to the frequency of the applied microwave radiation, $\nu_k$, to yield the fine-structure interval:

$$E_1-E_2=\nu_k-f[\nu_c(2^3S)]. \tag{30}$$

When fitting the data to Eq. (27) the parameter $C$ was rewritten as $[\nu_i(2^3P)-\nu_c]^2+(\gamma/2\pi)^2$. The true line shape contained four fitting parameters: $A$, $B$, $\gamma$, and $\nu_c$. In a line shape of this kind, however, there are only three independent quantities: the position of the center, the peak intensity, and the linewidth. The linewidth in this case depended on both $B$ and $\gamma$, which were closely correlated.

An iterative technique was used in applying the least-squares fitting procedure. Let the fitting parameters be designated by the set $x_j$. A set of trial values was adopted for the $x_j$. The "error" in signal, $\delta S_i$, for the $i$th point, due to the deviations $\delta x_j$ of the trial parameters from their best values, was expressed by a first-order Taylor expansion

$$\delta S_i=\sum_j\left(\frac{\partial S}{\partial x_j}\right)_i\delta x_j. \tag{31}$$

The differentials were, of course, obtained from the analytic expressions for the line shapes. The $\delta S_i$ were then compared with a set $\Delta S_i$, defined by

$$\Delta S_i=S_i(\text{expt.})-S_i(\text{theor.}). \tag{32}$$

$S_i$(expt.) is the observed signal for the $i$th point, and $S_i$(theor.) the value obtained by substituting $\nu_i(2^3P)$ into the analytic line shape using the trial parameters.

The expression $\sum_i(\delta S_i-\Delta S_i)^2$ was minimized to yield values for the $\delta x_j$. The least-squares procedure was straightforward since Eq. (31) is linear. A new set of trial parameters $(x_j+\delta x_j)$ was adopted and the procedure repeated until the values of the $(x_j+\delta x_j)$ converged. No difficulty was experienced in obtaining convergence for either of the line shapes in Eqs. (24′) and (27).

Typical examples of the fitted results are shown in Figs. 15(b) and 16(b), respectively, for a low-field and a high-field run. They correspond to the untreated data shown in Figs. 15(a) and 16(a). The fitted curves are based on Eq. (27), the true line shape.

### D. Error Analysis

A statistical error $\sigma_i$ was assigned to each measured signal point $S_i$(expt.). The value of $\sigma_i$ was based on the assumed validity of Poisson statistics for the number of detector counts over a given period. The theory of maximum likelihood[34] was applied to define an error matrix $H_{lm}$,

$$H_{lm}=\frac{1}{2}\frac{\partial^2 M}{\partial x_l\partial x_m}, \tag{33}$$

where $M$ is the least-squares sum,

$$M=\sum_i\frac{[S_i(\text{expt.})-S_i(\text{fitted})]^2}{\sigma_i^2}.$$

The $S_i$(fitted) are the values of $S_i$(theor.) using the best values of the fitting parameters $x_j$. The statistical uncertainties of the fitting parameters are then given by the square roots of diagonal elements of the inverse error matrix

$$\Delta x_l=(H_{ll}^{-1})^{1/2}. \tag{34}$$

The statistical uncertainty in the evaluation of the resonance center, $\Delta\nu_c$, was, as expected, roughly proportional to $\nu_{1/2}[S(\text{peak})]^{-1}[n-\beta]^{-1/2}$. $S$(peak) is the peak value of signal, $n$ is the number of points plotted,

[34] J. Orear, University of California Radiation Laboratory Report No. UCRL-9417, 1958 (unpublished): H. Cramer, *Mathematical Methods of Statistics* (Princeton University Press, Princeton, N. J., 1946).

TABLE I. Summary of all experimental runs on transition 4, $2^3P_2(M_J=0) \leftrightarrow 2^3P_1(M_J=0)$.

| Low field $(0 \rightarrow +1)$ trajectory | | | Low field $(0 \rightarrow -1)$ trajectory | | | High field $(0 \rightarrow +1)$ trajectory | | |
|---|---|---|---|---|---|---|---|---|
| Run No. | Result[a] | Weight | Run No. | Result[a] | Weight | Run No. | Result[a] | Weight |
| 7 | 0.186 | 15 | 1 | 0.206 | 2 | A | 0.175 | 54 |
| 8 | 0.218 | 7 | 2 | 0.198 | 3 | B | 0.199 | 104 |
| 9 | 0.158 | 19 | 4 | 0.214 | 4 | C | 0.208 | 77 |
| 10 | 0.183 | 15 | 5 | 0.173 | 3 | D | 0.244 | 18 |
| 11 | 0.212 | 16 | 6 | 0.163 | 6 | E | 0.198 | 59 |
| 12 | 0.229 | 5 | 10 | 0.199 | 10 | F | 0.199 | 23 |
| 13 | 0.215 | 11 | | | | G | 0.234 | 24 |
| 14 | 0.200 | 17 | | | | H | 0.195 | 148 |
| 15 | 0.202 | 11 | | | | I | 0.211 | 49 |
| 16 | 0.148 | 6 | | | | J | 0.176 | 45 |
| 17 | 0.189 | 73 | | | | K | 0.200 | 43 |
| 18 | 0.177 | 43 | | | | L | 0.196 | 28 |
| 19 | 0.188 | 9 | | | | M | 0.187 | 63 |
| 20 | 0.199 | 24 | | | | N | 0.184 | 73 |
| 21 | 0.165 | 14 | | | | O | 0.206 | 69 |
| 22 | 0.181 | 32 | | | | | | |
| 23 | 0.194 | 16 | | | | | | |
| 24 | 0.164 | 8 | | | | | | |
| 25 | 0.185 | 26 | | | | | | |
| 26 | 0.202 | 9 | | | | | | |
| 27 | 0.166 | 7 | | | | | | |
| 18 | 0.186 | 33 | | | | | | |
| 29 | 0.183 | 19 | | | | | | |
| 30 | 0.219 | 11 | | | | | | |
| 31 | 0.176 | 17 | | | | | | |
| 32 | 0.216 | 20 | | | | | | |
| 33 | 0.179 | 21 | | | | | | |
| Mean: 2291.188±0.004[b] MHz | | | Mean: 2291.191±0.009[b] MHz | | | Mean: 2291.197±0.004[b] MHz | | |

[a] Measured fine structure, $(E_1-E_2)=2291.0+$(result) MHz.
[b] Statistical standard deviations only; do not include systematic errors.

and $\beta$ is a positive constant approximately equal to the number of fitting parameters.

## VI. RESULTS

The results of all runs are summarized in Table I. Each run has been weighted by the value of $(1/\Delta\nu_c)^2$, since $\nu_c$ is the only parameter directly affecting the determination of the fine structure $E_1$-$E_2$. The over-all results for the $2^3P_1$-$2^3P_2$ fine structure were as follows:

low field: $E_1$-$E_2$=2291.188±0.015 MHz,

high field: $E_1$-$E_2$=2291.197±0.008 MHz,

weighted mean, all runs: $E_1$-$E_2$=2291.195±0.007 MHz.

The uncertainties quoted, intended to represent one standard deviation, are a combined estimate of the random and systematic errors.

The random error for each set of runs was the computed standard deviation of the grand mean. It arose in part from the statistical uncertainty related to the finite number of counts per point, and in part from random drifts and fluctuations in the signal intensity. The number of counts recorded per point was selected on the basis of roughly equalizing these two contributions to the random error.

Systematic errors in the low-field runs were ascribed primarily to the slope correction, and, to a lesser extent, the transition-5 correction. Their contribution to the quoted uncertainty was taken to be one third of the entire correction, which more than covered the discrepancy between the calculated and empirical corrections (see Sec. V A 1).

The major contributions to the errors for the high-field runs were the relativistic Zeeman corrections, since the uncertainty here was assumed to be one-half the entire correction. Uncertainties due to possible errors in the field measurements were somewhat smaller.

The agreement between the low- and high-field results was gratifying, in view of the entirely different natures of the sources of error involved in the two cases.

Our results are in good agreement with two independent, less accurate determinations of the $2^3P_1$-$2^3P_2$ separation. The first involved excitation of the $2^3P$ state by electron bombardment, and the detection of microwave resonances by observing the polarization of the decay radiation.[10] The result was

$$E_1-E_2=2291.42\pm0.36 \text{ MHz}.$$

The second determination was an optical level-crossing experiment[11] yielding

$$E_1-E_2=2291.200\pm0.022 \text{ MHz}.$$

## VII. DISCUSSION

Nonrelativistic variational wave functions have been applied to evaluate the theoretical fine structure.[12] The

result for the $2^3P_1-2^3P_2$ separation is 2289.59 MHz. This number contains a term due to the anomalous electron moment, and this is the only correction required of order $\alpha^3$ Ry.[35] Also included is a correction of 4.74 MHz (order $\alpha^4$ Ry) which arises from admixture of the $2^3P_1$ and $2^1P_1$ states by the spin-orbit interaction.[36] Other terms of order $\alpha^4$ Ry due to relativistic and radiative contributions remain to be evaluated, and these could quite easily account for the 1.61-MHz (7 parts in $10^4$) discrepancy between theory and experiment.

An experiment to measure the transition $2^3P_0(m_J=0)-2^3P_1(m_J=0)$ is currently in progress. We anticipate a precision of about 1 ppm for the $2^3P_0-2^3P_1$ fine-structure determination, the interval being about 29 617 MHz.[37] We are measuring in addition several $2^3P$ Zeeman transitions in magnetic fields up to 10 kG. These will enable us to measure the $g$ factors with an accuracy of 1 ppm, thereby yielding the relativistic and motional contributions to within 1%. These measurements, of intrinsic interest in themselves, should enable us to reduce substantially the uncertainties quoted above for the high field $2^3P_1$-$2^3P_2$ measurements. Experiments on the radiative lifetime of the $2^3P$ state and its hyperfine structure in the $He^3$ isotope are being completed.

## ACKNOWLEDGMENTS

Substantial contributions to the computations were made by Glenn Hollaway and Chung Pao Wu, whose assistance was sponsored in part by a National Science Foundation summer undergraduate program. It is a pleasure to acknowledge many fruitful and encouraging discussions with Professor W. E. Lamb, Jr., Professor W. Lichten, Professor P. A. Franken, and Professor G. Breit. We are grateful to Professor R. Serber for his permission to use unpublished material.

## APPENDIX A: TABLES OF ENERGY EIGENVALUES AND COUPLING COEFFICIENTS

In this Appendix we give in Tables II–IV, energy eigenvalues and coupling coefficients.

TABLE II. Secular matrix and energy eigenvalues for the states $^3P(\mathcal{J}m_J)$.

$\langle J',m_J'|\mathcal{H}|J,m_J\rangle$

$m_J=\pm2$:

$\langle 2,m_J|2,m_J\rangle=E_2+\frac{1}{2}\mu_0H(g_S+g_L)m_J$

$m_J=\pm1$:

| $J,m_J$ | $1,m_J$ | $2,m_J$ |
|---|---|---|
| $1,m_J$ | $E_1+\frac{1}{2}\mu_0H(g_S+g_L)m_J$ | $\frac{1}{2}\mu_0H(g_S-g_L)$ |
| $2,m_J$ | $\frac{1}{2}\mu_0H(g_S-g_L)$ | $E_2+\frac{1}{2}\mu_0H(g_S+g_L)m_J$ |

$m_J=0$:

| $J,m_J$ | 0,0 | 1,0 | 2,0 |
|---|---|---|---|
| 0,0 | $E_0$ | $(\frac{2}{3})^{1/2}\mu_0H(g_S-g_L)$ | 0 |
| 1,0 | $(\frac{2}{3})^{1/2}\mu_0H(g_S-g_L)$ | $E_1$ | $(\frac{1}{3})^{1/2}\mu_0H(g_S-g_L)$ |
| 2,0 | 0 | $(\frac{1}{3})^{1/2}\mu_0H(g_S-g_L)$ | $E_2$ |

Energy eigenvalues $W(\mathcal{J},m_J)$ found by diagonalizing the above matrices, where $E_0$, $E_1$, and $E_2$ are the zero-field energy eigenvalues; i.e., $E_J=\langle J,m_J|\mathcal{H}_{FS}|J,m_J\rangle$, $J=0$, 1, 2.

$W(2,\pm2)$: $E_2\pm(g_S+g_L)\mu_0H$

$W(2,\pm1)$: $\frac{1}{2}(E_1+E_2)\pm\frac{1}{2}(g_S+g_L)\mu_0H$
$-\frac{1}{2}[(E_1-E_2)^2+(g_S-g_L)^2(\mu_0H)^2]^{1/2}$

$W(1,\pm1)$: $\frac{1}{2}(E_1+E_2)\pm\frac{1}{2}(g_S+g_L)\mu_0H$
$+\frac{1}{2}[(E_1-E_2)^2+(g_S-g_L)^2(\mu_0H)^2]^{1/2}$

$W(2,0)$: $\frac{1}{2}(E_1+E_2)-\frac{1}{2}\{(E_1-E_2)^2+\frac{4}{3}(g_S-g_L)^2(\mu_0H)^2$
$\times[1+2(E_2-W(2,0))/(E_0-W(2,0))]\}^{1/2}$

$W(1,0)$: $\frac{1}{2}(E_1+E_2)+\frac{1}{2}\{(E_1-E_2)^2+\frac{4}{3}(g_S-g_L)^2(\mu_0H)^2$
$\times[1+2(E_2-W(1,0))/(E_0-W(1,0))]\}^{1/2}$

$W(0,0)$: $E_0+\dfrac{\frac{2}{3}(W(0,0)-E_2)(g_S-g_L)^2(\mu_0H)^2}{[(W(0,0)-E_1)(W(0,0)-E_2)-\frac{1}{3}(g_S-g_L)^2(\mu_0H)^2]}$

TABLE III. The coefficients $(Jm|\mathcal{J}m)$. [Note $(Jm|\mathcal{J}m')=0$ when $m\neq m'$.] The transition frequencies are given by[a]
(4) $(1,0)\leftrightarrow(2,0)$: $\nu_4=(E_1-E_2)+\frac{2}{3}h^2\{(E_1-E_2)^{-1}-(E_0-E_1)^{-1}\}$,
(5) $(1,\pm1)\leftrightarrow(2,\pm1)$: $\nu_5=(E_1-E_2)\{1+h^2(E_1-E_2)^{-2}\}^{1/2}$.

| $\mathcal{J},m$ \ $J,m$ | 0,0 | 1,0 | 2,0 | 1,±1 | 2,±1 | 2,±2 |
|---|---|---|---|---|---|---|
| 0,0[a] | $[1+2h^2/3(E_0-E_1)^2]^{-1/2}$ | $(\frac{2}{3})^{1/2}h[(E_1-E_0)^2+\frac{2}{3}h^2]^{-1/2}$ | 0 | 0 | 0 | 0 |
| 1,0[b] | $-(\frac{2}{3})^{1/2}hB/(E_0-E_1)$ | $B$ | $(\frac{1}{3})^{1/2}hB/(E_1-E_2)$ | 0 | 0 | 0 |
| 2,0 | 0 | $-(\frac{1}{3})^{1/2}h[(E_1-E_2)^2+\frac{1}{3}h^2]^{-1/2}$ | $[1+h^2/3(E_1-E_2)^2]^{-1/2}$ | 0 | 0 | 0 |
| 1,±1[c] | 0 | 0 | 0 | $C$ | $hC/2(E_1-E_2)$ | 0 |
| 2,±1[c] | 0 | 0 | 0 | $-hC/2(E_1-E_2)$ | $1/C$ | 0 |
| 2,±2 | 0 | 0 | 0 | 0 | 0 | 1 |

[a] $h=(g_S-g_L)\mu_0H$. [b] $B=[1+2h^2/3(E_0-E_1)^2+h^2/3(E_1-E_2)^2]^{-1/2}$. [c] $C=[1+h^2/4(E_1-E_2)^2]^{-1/2}$.

[35] H. Araki, Progr. Theoret. Phys. (Kyoto) **17**, 619 (1957); J. Sucher, Phys. Rev. **109**, 1010 (1958).
[36] G. Araki, M. Ohta, and K. Mano, Phys. Rev. **116**, 651 (1959).
[37] J. Lifsitz and R. H. Sands (Ref. 11); C. E. Johnson, F. M. J. Pichanick, A. Kponou, S. A. Lewis, and V. W. Hughes, Bull. Am. Phys. Soc. **13**, 20 (1968).

TABLE IV. Values of the coefficients $\{m_S m_L|\mathcal{J}m_J\}^2$ to first order in the field.[a]

| $\mathcal{J},m_J$ \ $m_S,m_L$ | (1,1) | (1,0) | (1,−1) | (0,1) | (0,0) | (0,−1) | (−1,1) | (−1,0) | (−1,−1) |
|---|---|---|---|---|---|---|---|---|---|
| 0,0 | 0 | 0 | $\frac{1}{3}\left[1+\frac{2h}{(E_0-E_1)}\right]$ | 0 | $\frac{1}{3}$ | 0 | $\frac{1}{3}\left[1-\frac{2h}{(E_0-E_1)}\right]$ | 0 | 0 |
| 1,0 | 0 | 0 | $\frac{1}{2}\left[1+\frac{2h}{3(E_1-E_2)}-\frac{4h}{3(E_0-E_1)}\right]$ | 0 | 0 | 0 | $\frac{1}{2}\left[1-\frac{2h}{3(E_1-E_2)}+\frac{4h}{3(E_0-E_1)}\right]$ | 0 | 0 |
| 2,0 | 0 | 0 | $\frac{1}{6}\left[1-\frac{2h}{(E_1-E_2)}\right]$ | 0 | $\frac{2}{3}$ | 0 | $\frac{1}{6}\left[1+\frac{2h}{(E_1-E_2)}\right]$ | 0 | 0 |
| 1,±1 | 0 | $\frac{1}{2}\left[1-\frac{h}{(E_1-E_2)}\right]$ | 0 | $\frac{1}{2}\left[1+\frac{h}{(E_1-E_2)}\right]$ | 0 | $\frac{1}{2}\left[1+\frac{h}{(E_1-E_2)}\right]$ | 0 | $\frac{1}{2}\left[1-\frac{h}{(E_1-E_2)}\right]$ | 0 |
| 2,±1 | 0 | $\frac{1}{2}\left[1+\frac{h}{(E_1-E_2)}\right]$ | 0 | $\frac{1}{2}\left[1-\frac{h}{(E_1-E_2)}\right]$ | 0 | $\frac{1}{2}\left[1-\frac{h}{(E_1-E_2)}\right]$ | 0 | $\frac{1}{2}\left[1+\frac{h}{(E_1-E_2)}\right]$ | 0 |
| 2,±2 | 1 | 0 | 0 | 0 | 0 | 0 | 0 | 0 | 1 |

[a] $h=(g_S-g_L)\mu_0 H$; for $\pm m_J$ entries are nonzero only if $m_J=m_S+m_L$.

## APPENDIX B: DERIVATION OF EQS. (12) AND (24)

We summarize here the unpublished calculation of Serber.[24] This calculation is a perturbation treatment of the atom in the presence of external optical and microwave radiation, and the results therefrom justify our using Eqs. (12) and (24) in the analysis of our data.

Several assumptions are made during the course of the calculation. Some of these assumptions are merely for computational convenience and do not affect the nature of the final result. The quantities of interest and their approximate magnitudes in our case are as follows:

(a) the widths of the excited levels, $\gamma\sim 3$ MHz;

(b) the frequencies of the excitation and decay photons, $k\sim 3\times 10^8$ MHz;

(c) the excitation rate of the lower levels, $\sigma\sim 0.01$ MHz;

(d) the spectral width of the incident radiation, $\Delta k\sim 10^4$ MHz;

(e) the frequency of the applied rf field, $\omega/2\pi\sim 2\times 10^3$ MHz.

The assumptions are as follows:

(I) $\gamma\ll k$;

(II) $\omega,\ \Delta k\ll k$;

(III) $\sigma\ll\gamma\ll\Delta k$;

(IV) $\sigma\ll\omega$.

In general the notation of Sec. II will be employed, except that the $\mathcal{J}m_J$ for an excited level will be abbreviated to $m$. In addition, we shall write the zero-order energies of the initial ($m_S$), excited ($m$), and final ($m_S'$) states as $\omega_0$, $\omega_m$, and $w_f$, respectively. It is assumed that $m$ is excited with the absorption of a photon $\mathbf{k}$ with energy $k$, and that $m_S'$ is reached after absorption of a photon $\mathbf{k}$ and emission of a photon $\mathbf{k}'$. The relevant time-dependent amplitudes are $b(m_S;t)$, $b(m,-\mathbf{k};t)$, and $b(m_S',-\mathbf{k},\mathbf{k}';t)$.

The optical-excitation operator $\mathcal{J}_{\rm op}$ and the rf magnetic field operator $\mathbf{V}$ are regarded as perturbations on the system free-atom–plus–radiation-field, and the solutions to the zero-order (time-independent) Schrödinger equation are assumed known. Radiative decay is represented by an operator $\mathbf{\Gamma}$, analogous to $\mathcal{J}_{\rm op}$. The time-dependent Schrödinger equation for the perturbed system is written, and a set of coupled differential equations is obtained in the usual way for the time-dependent amplitudes. The solutions are assumed to be quasiperiodic [assumption (III)], and hence the final-state amplitudes are written in the form

$$b(m_S',-\mathbf{k},\mathbf{k}';t)=e^{-i(\omega_0+u_0)t}b(m_S';t). \qquad \text{(B1)}$$

The quantity $u_0$ remains to be determined. The real part of $u_0$ is the change in energy of the initial state ($m_S$) due to the applied radiation (light shift). The

imaginary part $i\sigma_0$ is the width of the state and depends on the rate of excitation.

Time-dependent coefficients for the initial and excited states are defined in terms of the quasiperiodic solutions

$$b(m_S;t)=e^{-i(\omega_0+u_0)t}\sum_r b(m_S,r)e^{ir\omega t},$$
$$b(m,-\mathbf{k};t)=e^{-i(\omega_0+u_0)t}\sum_r b(m,r)e^{ir\omega t}, \tag{B2}$$

where $\omega$ is the frequency of the applied rf field and $r$ is a positive (negative) integer representing the number of rf photons emitted (absorbed).

The set of differential equations becomes

$$-\sum_r (r\omega-u_0)b(m_S,r)e^{ir\omega t}=\sum_{r,m}\int\langle m_S|\mathbf{\Gamma}(\mathbf{k})|m\rangle b(m,r)e^{ir\omega t}d\mathbf{k}, \tag{B3a}$$

$$-\sum_r(\omega_m-\omega_0-k+r\omega-u_0)b(m,r)e^{ir\omega t}=\sum_{r,m'}[\langle m|\mathbf{V}|m'\rangle e^{i\omega t}+\langle m|\mathbf{V}^\dagger|m'\rangle e^{-i\omega t}]\times b(m',r)e^{ir\omega t}+\sum_r\langle m|g_{\rm op}(\mathbf{k})|m_S\rangle b(m_S,r)e^{ir\omega t}+\sum_{m_S'}\int\langle m|g_{\rm op}(\mathbf{k}')|m_S'\rangle b(m_S';t)d\mathbf{k}', \tag{B3b}$$

$$ib(m_S';t)-(\omega_f-\omega_0-k+k'-u_0)b(m_S';t)=\sum_{r,m}\langle m_S'|\mathbf{\Gamma}(\mathbf{k}')|m\rangle b(m;r)e^{ir\omega t}. \tag{B3c}$$

The scattering of more than one photon can be treated if necessary by additional terms in Eq. (B3c).

Equation (B3c) is integrated to give an expression for the $b(m_S';t)$ in terms of the $b(m;r)$. This is substituted into the last term of Eq. (B3b), which is integrated to yield

$$\sum_{m_S'}\int\langle m|g_{\rm op}(\mathbf{k}')|m_S'\rangle b(m_S';t)d\mathbf{k}'=\sum_{r,m'}W(m,m';r)b(m',r)e^{ir\omega t}, \tag{B4}$$

where $W(m,m';r)$ is the value of the integral over $d\mathbf{k}'$, obtained by disregarding transient contributions [assumption (III)]. It represents the effects of the radiation fields on the levels $m, m'$. The real part of $W(m,m';r)$ gives the shifts of these levels in the presence of the radiation, while the imaginary part gives their widths under induced and spontaneous emission. The spontaneous emission terms are diagonal in $m$, and the partial width for spontaneous decay to a final state $m_S'$ is given by

$$\gamma(m,m_S';k,r)=\pi\int\frac{1}{2}|\langle m|\mathbf{\Gamma}(\mathbf{k}')|m_S'\rangle|^2\times\delta(\omega_0-\omega_f+u_0-u_f-k+k'+r\omega)d\mathbf{k}'. \tag{B5}$$

The dependence on $r$ and $k$ may be neglected [assumption (II)], and Eq. (B5) becomes the partial decay rate $\gamma(m,m_S')$.[38]

It is convenient to define

$$\begin{aligned}&\omega_0'=\omega_0+u_0,\\&\omega_f'=\omega_f+u_f,\\&\omega_m'=\omega_m+W(m,m';r)\sim\omega_m+W(m,m';0),\\&\omega_{m0}'=\omega_m'-\omega_0',\\&\omega_{mf}'=\omega_m'-\omega_f',\\&\omega_{f0}'=\omega_f'-\omega_0'.\end{aligned} \tag{B6}$$

Equating coefficients of $e^{ir\omega t}$ in Eq. (B3b) one obtains

$$-(\omega_{m0}'-k+r\omega)b(m,r)=\sum_{m\neq m'}W(m,m';r)b(m',r)+\sum_{m'}\langle m|\mathbf{V}|m'\rangle b(m',r-1)+\sum_{m'}\langle m|\mathbf{V}^\dagger|m'\rangle\times b(m',r+1)+\langle m|g_{\rm op}(\mathbf{k})|m_S\rangle b(m_S,r). \tag{B7}$$

The factor $(r\omega-u_0)$ on the left-hand side of Eq. (B3a) suggests that $b(m_S,0)$ is much larger than the $b(m_S,r)$ for $r\neq0$ [assumption (IV)]. Furthermore, in Eq. (B7), $b(m,0)$ is appreciable only when $k\sim\omega_{m0}'$ (i.e., resonant excitation of $m$). Thus in the excitation process $b(m_S,0)$ acts as a source for $b(m,0)$, which in turn acts as a source for $b(m',\pm r)$ in the rf resonant process. We label as $\alpha$, $\beta$ the states $m$, $m'$ of interest (see Sec. II), and consider the case involving one rf photon near resonance: $\omega\sim\omega_{\alpha\beta}'$. All other excited-state amplitudes for $m$, $m'\neq\alpha$, $\beta$ can be neglected if one allows for the Bloch-Siegert effect (Sec. V A 4) by replacing $\omega_{\alpha\beta}'$ with

$$\omega_{\alpha\beta}''=\omega_{\alpha\beta}'+(\text{Bloch-Siegert shift}). \tag{B8}$$

Equations (B7) reduce to

$$\begin{aligned}(\omega_{\alpha0}''-k)b(\alpha,0)+\langle\alpha|\mathbf{V}|\beta\rangle b(\beta,-1)&=-\langle\alpha|g_{\rm op}(\mathbf{k})|m_S\rangle b(m_S,0),\\(\omega_{\beta0}''-\omega-k)b(\beta,-1)+\langle\beta|\mathbf{V}|\alpha\rangle b(\alpha,0)&=0.\end{aligned} \tag{B9}$$

[38] This differs from the $\gamma(m,m_S')$ in Sec. II, where they were defined so that $\sum_{m_S'}\gamma(m,m_S')=1$. In this case $\sum_{m_S'}\gamma(m,m_S')=\gamma$, the total width of the state $m$.

The solutions are

$$b(\alpha,0)=-\frac{\langle\alpha|\mathcal{J}_{\rm op}(\mathbf{k})|m_S\rangle(\omega_{\alpha 0}''+\omega_{\alpha+}+\omega_{\alpha-}-k)}{(k-\omega_{\alpha 0}''-\omega_{\alpha+})(k-\omega_{\alpha 0}''-\omega_{\alpha-})}\times b(m_S,0), \quad \text{(B10a)}$$

$$b(\beta,-1)=\frac{\langle\alpha|\mathcal{J}_{\rm op}(\mathbf{k})|m_S\rangle\langle\beta|\mathbf{V}|\alpha\rangle}{(k-\omega_{\alpha 0}''-\omega_{\alpha+})(k-\omega_{\alpha 0}''-\omega_{\alpha-})}b(m_S,0), \quad \text{(B10b)}$$

with

$$\omega_{\alpha\pm}=\tfrac{1}{2}(\omega_{\alpha\beta}''-\omega)\pm\tfrac{1}{2}[(\omega_{\alpha\beta}-\omega)^2+4|\mathbf{V}|^2]^{1/2}, \quad \text{(B11a)}$$

where we have abbreviated $|\langle\beta|\mathbf{V}|\alpha\rangle|^2$ by $|\mathbf{V}|^2$. Similarly,

$$b(\beta,0)=-\frac{\langle\beta|\mathcal{J}_{\rm op}(\mathbf{k})|m_S\rangle(\omega_{\beta 0}''+\omega_{\beta+}+\omega_{\beta-}-k)}{(k-\omega_{\beta 0}''-\omega_{\beta+})(k-\omega_{\beta 0}''-\omega_{\beta-}'')}\times b(m_S,0), \quad \text{(B10c)}$$

$$b(\alpha,1)=\frac{\langle\beta|\mathcal{J}_{\rm op}(\mathbf{k})|m_S\rangle\langle\alpha|\mathbf{V}|\beta\rangle}{(k-\omega_{\beta 0}''-\omega_{\beta+})(k-\omega_{\beta 0}''-\omega_{\beta-}'')}b(m_S,0), \quad \text{(B10d)}$$

$$\omega_{\beta\pm}=-\tfrac{1}{2}(\omega_{\alpha\beta}''-\omega)\pm\tfrac{1}{2}[(\omega_{\alpha\beta}''-\omega)^2+4|\mathbf{V}|^2]^{1/2}. \quad \text{(B11b)}$$

These expressions for the amplitudes of $\alpha$ and $\beta$, together with analogous terms for excited states not coupled by the rf field, are now inserted into Eq. (B3a) to yield $u_0$. The total rate of excitation from $m_S$ is given by the imaginary part of $u_0$:

$$\sigma(m_S)=\pi\sum_{m\neq\alpha,\beta}\int|\langle m|\mathcal{J}_{\rm op}(\mathbf{k})|m_S\rangle|^2\delta(k-\omega_{m0}'')d\mathbf{k}+\sum_{m'=\alpha,\beta}\left[\frac{-\omega_{m'-}}{\omega_{m'+}-\omega_{m'-}}\sigma^+(m_S,m')+\frac{\omega_{m'+}}{\omega_{m'+}-\omega_{m'-}}\sigma^-(m_S,m')\right], \quad \text{(B12)}$$

where the partial excitation rates are given by

$$\sigma^\pm(m_S,m')=\pi\int|\langle m'|\mathcal{J}_{\rm op}(\mathbf{k})|m_S\rangle|^2\times\delta(k-\omega_{m'0}''-\omega_{m'\pm})d\mathbf{k}. \quad \text{(B13)}$$

The terms $\omega_{\alpha\pm}$, $\omega_{\beta\pm}$ are of order $\omega_{\alpha\beta}''$, and the replacement

$$\sigma^\pm(m_S,m')=\sigma(m_S,m')=\pi\int|\langle m'|\mathcal{J}_{\rm op}(\mathbf{k})|m_S\rangle|^2\times\delta(k-\omega_{m'0}'')d\mathbf{k} \quad \text{(B14)}$$

merely assumes that the incident-light spectrum changes little over a range $\omega_{m'+}-\omega_{m'-}$.

The probability $P(m_S\rightarrow m_S')$, that an atom reaches the state $m_S'$ at time $t$ is given by

$$P(m_S\rightarrow m_S')=\int\int|b(m_S',-\mathbf{k},\mathbf{k}';t)|^2d\mathbf{k}d\mathbf{k}'=\int|b(m_S';t)|^2d\mathbf{k}'e^{-2\sigma(m_S)t}, \quad \text{(B15)}$$

from Eq. (B1).

The integrated form of Eq. (B3c) is substituted into Eq. (B15), using Eqs. (B10) for the excited-state amplitudes. Integration of Eq. (B15) then yields

$$P(m_S\rightarrow m_S')=\frac{1}{\gamma}\Big\{\sum_m\gamma(m,m_S')\sigma(m_S,m)+\{\gamma(\beta,m_S')-\gamma(\alpha,m_S')\}\{\sigma(m_S,\alpha)-\sigma(m_S,\beta)\}\times\frac{2|\mathbf{V}|^2}{(\omega_{\alpha\beta}''-\omega)^2+\gamma^2+4|\mathbf{V}|^2}\Big\}\frac{e^{-2\sigma(m_S)t}-e^{-2\sigma(m_S')t}}{\sigma(m_S')-\sigma(m_S)}. \quad \text{(B16)}$$

It has been assumed that $|b(m_S,0)|^2$ is unity, since it differs from unity by terms of order $\sigma(m_S)/\gamma$. Equation (B16) is completely equivalent to Eqs. (12) and (24) in Sec. II, if one remembers the different normalizations of $\sigma$ and $\gamma$. The time-dependent factor in Eq. (B16) arises because the expression involves a time-dependent probability, whereas in Eq. (12) we have a probability per process of excitation and decay.

## APPENDIX C: CORRECTIONS TO THE ZEEMAN EFFECT

### 1. Motional Corrections

The contribution of the orbital magnetic moment to the Zeeman Hamiltonian equation (1) is[17]

$$\mathbf{Z}_l=\frac{\mu_0}{\hbar}H_z\Big\{\Big(1-\frac{m}{M}\Big)\sum_i(\mathbf{r}_i\times\mathbf{p}_i)_z-\frac{m}{M}\sum_{i<j}[(\mathbf{r}_i\times\mathbf{p}_j)_z+(\mathbf{r}_j\times\mathbf{p}_i)_z]\Big\}, \quad \text{(C1)}$$

where $H_z$ is the external magnetic field, $\mu_0$ is the Bohr magneton, $m$ and $M$ are, respectively, the masses of the electron and the nucleus, and $\mathbf{r}_i$ and $\mathbf{p}_i$ are, respectively, the coordinate and momentum operators for the $i$th electron.

The first term in braces is proportional to the $z$ component of $\mathbf{L}$, the total orbital-angular-momentum operator. In order to evaluate the second term we have expressed $\mathbf{r}_i\times\mathbf{p}_j$ in the form

$$\mathbf{r}_i\times\mathbf{p}_j=\frac{2r_i}{r_j}\{\mathbf{C}_i^{(1)}(\mathbf{C}_j^{(1)}\mathbf{l}_j)^{(1)}\} -r_i\frac{\partial}{\partial r_j}\sqrt{2}\{\mathbf{C}_i^{(1)}\mathbf{C}_j^{(1)}\}^{(1)}, \quad \text{(C2)}$$

where $\mathbf{C}_i^{(1)}$ is the first-rank spherical tensor operator for the $i$th electron, and $\mathbf{l}_j$ is the orbital-angular-momentum operator for the $j$th electron. Tensor products have been expressed in the usual way.[39] The angular parts of the matrix elements of Eq. (C2) between $^3Pm_J$ states are also proportional to those of $L_z$. Hence the entire motional effect can be incorporated into a corrected value $g_L'$ of the orbital $g$ factor:

$$\mathbf{Z}_l=(\mu_0/\hbar)g_L'H_z. \quad \text{(C3)}$$

We have evaluated the radial integrals in Eq. (C2) using an antisymmetrized product of $1s$, $2p$ hydrogenic wave functions, with effective nuclear charges $Z(1s)=1.99$ and $Z(2p)=1.09$, with the result

$$g_L'=0.999872. \quad \text{(C4)}$$

### 2. Relativistic Corrections

If the Zeeman Hamiltonian is written in the form

$$\mathbf{Z}=\boldsymbol{\mu}\cdot\mathbf{H}=\mu_zH_z,$$

then the relativistic contributions to the Zeeman Hamiltonian can be written as corrections to the magnetic-moment operators in the forms[16]

$$\begin{aligned}\delta\boldsymbol{\mu}_{1,2}&=-\alpha^2\mu_0\sum_i\{(\mathbf{l}_i+2\mathbf{s}_i)T_i-\tfrac{1}{2}Z[\mathbf{s}_i\times\boldsymbol{\nabla}_i(r_i^{-1})]\times\mathbf{r}_i\},\\ \delta\boldsymbol{\mu}_{3,4}&=-\alpha^2\mu_0\sum_{i<j}[(\mathbf{s}_i+2\mathbf{s}_j)\times\boldsymbol{\nabla}_i(r_{ij}^{-1})]\times\mathbf{r}_i,\\ \delta\boldsymbol{\mu}_5&=-\alpha^2\mu_0\sum_{i<j}[r_{ij}^{-1}(\mathbf{r}_i\times\mathbf{p}_j)+r_{ij}^{-3}(\mathbf{r}_i\times\mathbf{r}_j)(\mathbf{r}_{ij}\cdot\mathbf{p}_j)],\end{aligned} \quad \text{(C5)}$$

where $\alpha$ is the fine-structure constant, $\mathbf{l}_i$ and $\mathbf{s}_i$ are, respectively, the orbital and spin angular-momentum operators for the $i$th electron, $T_i$ is the kinetic-energy operator for the $i$th electron, and $\mathbf{r}_i(\mathbf{r}_j)$ is the spatial coordinate operator for the $i$th($j$th) electron with $\mathbf{r}_{ij}=\mathbf{r}_j-\mathbf{r}_i$.

Innes and Ufford[16] have recoupled Eqs. (C5) in spherical tensor form. We have used their results, together with the hydrogenic approximation for the radial wave functions, to obtain the $2^3P$, $m_J=0$ matrix elements which are relevant to our measurement of transition 4:

$$\begin{aligned}&&\delta\mu_{1,2}&&\delta\mu_{2,3}&&\delta\mu_5\\ \langle 2^3P_1,m_J=0|(\delta\mu)_z|2^3P_2,m_J=0\rangle&=(&-67.0&&-4.0&&+0.4)\times(\tfrac{1}{3})^{1/2}\mu_0\times10^{-6},\\ \langle 2^3P_1,m_J=0|(\delta\mu)_z|2^3P_0,m_J=0\rangle&=(&-63.0&&-9.9&&+0.4)\times(\tfrac{2}{3})^{1/2}\mu_0\times10^{-6}.\end{aligned} \quad \text{(C6)}$$

These corrections were incorporated into our data reduction by including the above matrix elements in the secular equation for $m_J=0$ (see Table II). It can be seen that the predominant contribution arises from the term $\delta\mu_{1,2}$. The radial integrals involved in this term are of the type $\langle r_i^{-1}\rangle$ and $\langle T_i\rangle$, and the accuracy of these could be checked from the known total energy of the $2^3P$ state. This comparison indicates that the accuracy of our result for $\delta\mu_{1,2}$, which contributes 7 ppm to the measured (high-field) $2^3P$ fine structure, should be more than adequate. The total contribution of the above values for $\delta\mu_{3,4}$ and $\delta\mu_5$ is only 0.5 ppm, but because these terms contain several complex radial integrals which could not be checked, we have allowed an uncertainty of 2 ppm in our quoted result.

[39] See, for instance, B. R. Judd, *Operator Techniques in Atomic Spectroscopy* (McGraw-Hill Book Co., New York, 1963).